

Flowing Fast and Slow

Interactions Between Fast and Slow Dynamics in Nonlinear Evolution Equations

Thomas M. Hodgson, Kieran Quaine, Jonna C. Roden
Maxwell Institute

December 18, 2018

Contents

1	Introduction	1
2	Standard Theory for Fast-Slow Systems and Where It Fails	4
2.1	Reduced Dynamics	4
2.2	Geometric Singular Perturbation Theory	5
2.3	Fold Points	7
2.4	The Van der Pol System: GSPT and Fold Points	7
3	The Blow-Up Method	9
3.1	Coordinate Transformation and Charts	9
3.2	Dynamics in K_2	11
3.3	Dynamics in K_1	13
3.4	Dynamics in K_3	17
3.5	The Full Solution	20
4	Canards in Two Dimensions	21
4.1	The Blow-Up Method on the Canard Point	24
4.1.1	Dynamics in K_2	26
4.1.2	Dynamics in K_1	27
4.2	Full Solution	29
4.3	Effect of the Canard Point	29
4.3.1	Separation of the Manifolds	32
5	Canards in Three Dimensions	34
5.1	The Folded Node	38
6	Global Return Mechanisms and Mixed Mode Oscillations	43
6.1	The Folded Node	43
6.2	Singular Hopf Bifurcation	45
7	Discussion	47
8	Acknowledgements	47
8.1	Author Contribution	47
A	Numerical Simulation	49
A.1	Stiff Solvers	50

List of Figures

1	Examples of fast-slow systems in nature.	2
2	Van der Pol Dynamics with $\epsilon = 1$	3
3	Van der Pol Dynamics with $\epsilon = 0.01$	3
4	Three charts mapping different sections of our blow up (?).	10
5	Phase portrait for chart 2 (?).	11
6	Riccati solution for chart 2 (?).	13
7	Dynamics in chart 1 (?).	14
8	The full solution associated with the flow on the fold point.	21
9	The reduced flow where a) $\lambda = 0$ and b) $\lambda > 0$	22
10	Example trajectories for varying λ	22
11	The Van der Pol system for the canard case.	25
12	Full dynamics at the fold point in the canard case (?).	29
13	The trajectories associated with the canards case of the Van der Pol system.	31
14	Separation of M_a and M_r (?).	32
15	Three dimensional Van der Pol (?).	35
16	Phase portraits around singularities	37
17	The branches of a spiral (?).	37
18	Local dynamics around the folded node for $\mu \approx 0.0557$ (?).	42
19	Orbits associated with mixed mode oscillations (?).	46
20	Numerical Stability Comparison	51
21	Stiff Solvers	52

Abstract

This project will be considering the Fast-Slow dynamics in non-linear ordinary differential equations. The aim is to introduce techniques required to analyse a system in full detail. The main obstruction will be the existence of singular points within the system, so called fold points. These cause standard Geometric Singular Perturbation Theory to fail, so alternative methods are required to explain the global dynamics. We discuss the blow-up method by which we are, in essence, magnifying the fold point to find the flow in this region. The results of this can be seen throughout the report as we would expect periodic solutions or jumps within the system. The method is then applied to the Van der Pol system, whereby we consider the case for $\lambda = 1$ and $\lambda > 0$ – leading to a jump point for the former and the formation of a canard solution in the latter case. Three dimensional systems and Mixed Mode Oscillations (MMOs) are introduced and we consider the dynamics around a folded node and briefly discuss the existence of singular Hopf bifurcations for a folded saddle.

1 Introduction

Nonlinear evolution equations are ubiquitous across the sciences. These typically take the form,

$$\dot{x}(t) = F(x(t)),$$

where $x \in \mathbf{R}^d, F \in C^r(\mathbf{R}^d, \mathbf{R}^d)$. We will be interested in systems that occur on different timescales, known as fast-slow systems. These occur naturally in physics, neuroscience and many other biological scenarios (???). Models of such systems can be written generally in the form,

$$\begin{cases} x' &= \frac{dx}{dt} = f(x, y, \epsilon), \\ y' &= \frac{dy}{dt} = \epsilon g(x, y, \epsilon), \end{cases} \quad (1)$$

Here, $x \in \mathbf{R}^n, y \in \mathbf{R}^m, m, n \geq 1$ and f, g are sufficiently smooth. The separation in timescales is governed by $0 < \epsilon \ll 1$, known as the timescale separation parameter. Some systems also act on more than two timescales, in which case there is more than one timescale separation parameter. In the system above, note that the change in x is $O(1)$, whilst it is $O(\epsilon)$ in y . As ϵ is very small, this means that the change in x is much faster than that of y . If we slow down time with the transformation $\tau = \epsilon t$, the system becomes

$$\begin{cases} \epsilon \dot{x} &= \epsilon \frac{dx}{d\tau} = f(x, y, \lambda, \epsilon), \\ \dot{y} &= \frac{dy}{d\tau} = g(x, y, \lambda, \epsilon), \end{cases} \quad (2)$$

Represented like this, $\dot{x} = O(\frac{1}{\epsilon})$ whilst $\dot{y} = O(1)$. The time scale given by τ is said to be slow so (2) is the *slow system* while (1) is the *fast system*.

Throughout, the motivating example will be the Van der Pol equation. The Van der Pol oscillator is a well-studied second order ODE that is used to model a variety of physical and biological phenomena.

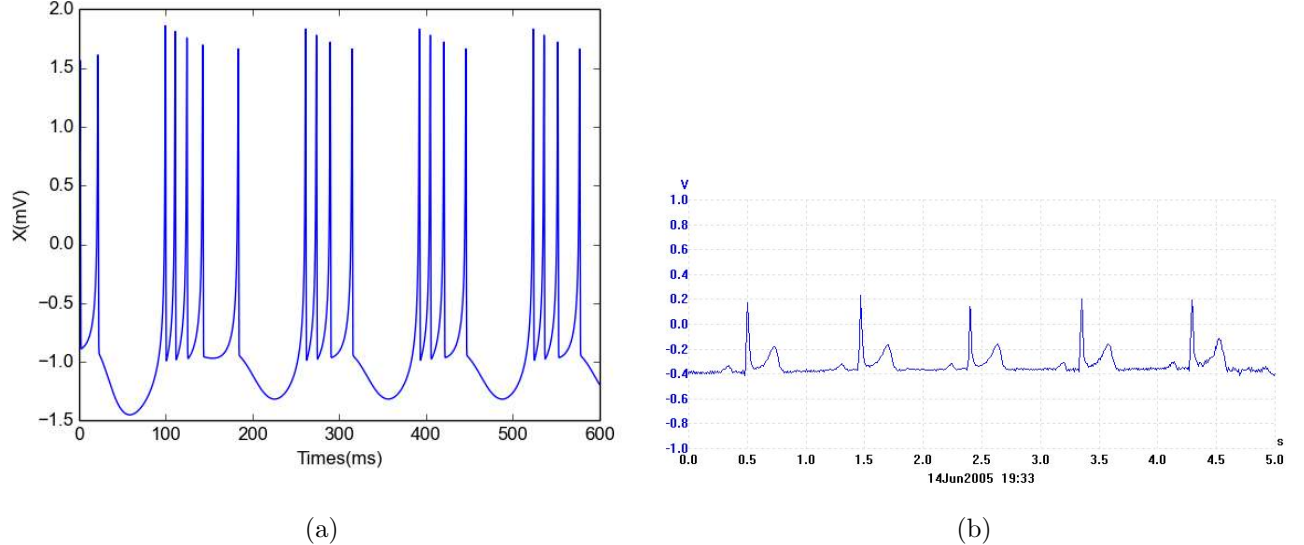


Figure 1: Examples of fast-slow systems in nature. a) The Hindmarsh-Rose model of a neuron (?) and b) An electrocardiogram trace of a heart beat (?)

It was developed by the Dutch physicist and electrical engineer Balthasar Van der Pol, who conducted research on electrical circuits. It describes the evolution of the position coordinate $x(t)$ according to the following the ODE,

$$\ddot{x}(t) - \mu(1 - x^2(t))\dot{x}(t) + x(t) = 0, \quad (3)$$

where $\mu \gg 1$ is a scalar constant. This equation can be scaled so that it becomes a two dimensional fast-slow system of the form shown in Equation (1) after a change of variables,

$$\begin{cases} x' = -y + x^2 - \frac{x^3}{3}, \\ y' = \epsilon(-\lambda + x). \end{cases} \quad (4)$$

When presented with any dynamical system, the aim is to fully understand the global dynamics of the system. A numerical simulation is often a good first step. Setting $\lambda = \epsilon = 1$ gives the phase plane given in Figure 2. Figure 2 shows the presence of a periodic large amplitude oscillation, which Van der Pol called *relaxation oscillations*. Setting $\epsilon = 1$ means that there is no separation in timescale. Figure 3 shows a more realistic scenario, when $\epsilon = 0.01$. Here there is what appears to be an almost instantaneous change in x every 800 time steps. What causes this rapid change? We wish to find a rigorous reason for this jump from slow to fast movement. A natural starting point would be to study what happens when $\epsilon = 0$, that is, when this rapid change is in fact instantaneous. Doing so in both the fast and slow system will give two different views of the dynamics. Taking the limit $\epsilon \rightarrow 0$ in the fast system (1) gives,

$$\begin{cases} x' = \frac{dx}{dt} = f(x, y, \lambda, \epsilon), \\ y' = 0. \end{cases} \quad (5)$$

1. INTRODUCTION

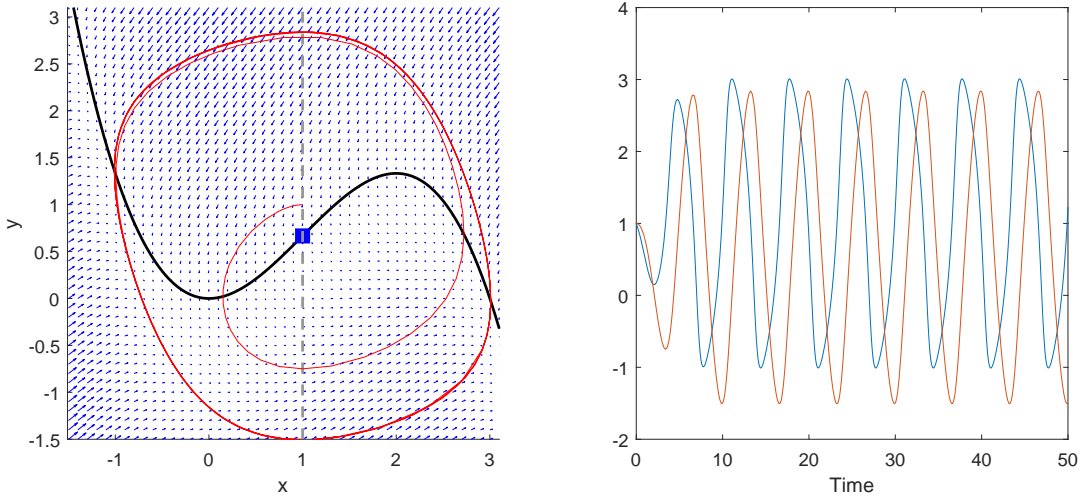


Figure 2: Phase plane and time series of the Van der Pol for $\epsilon = \lambda = 1$ started from $(1, 1)$. The dashed line indicates the null cline in y while that in x is given by the solid black line. The equilibrium is highlighted in blue.

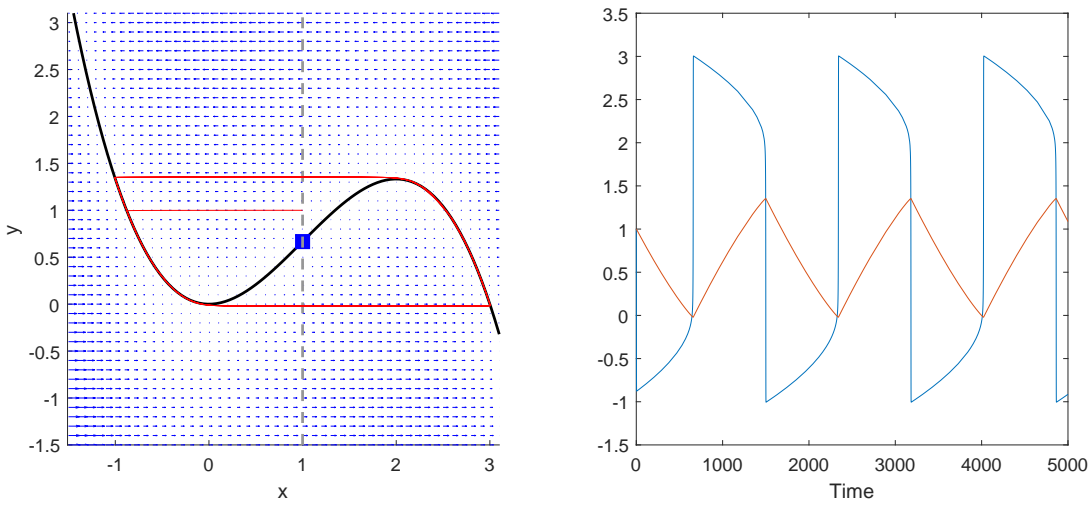


Figure 3: Phase plane and time series of the Van der Pol for $\epsilon = 0.01, \lambda = 1$ started from $(1, 1)$. The dashed line indicates the null cline in y while that in x is given by the solid black line. The equilibrium is highlighted in blue.

This is known as the *layer problem* as movement is restricted to the layers $y = \text{const.}$ and similarly taking the limit in the slow system (2) gives,

$$\begin{cases} 0 &= \epsilon \frac{dx}{d\tau} = f(x, y, \lambda, 0), \\ \dot{y} &= \frac{dy}{d\tau} = g(x, y, \lambda, 0). \end{cases} \quad (6)$$

This is known as the *reduced problem* as the dynamics are reduced from the whole plane to the manifold $f = 0$. In the Van der Pol system, $f(x, y, \lambda, \epsilon) = -y + x^2 + \frac{x^3}{3}$ and $g(x, y, \lambda, \epsilon) = -\lambda + x$. Then the set,

$$S = \{(x, y) : f(x, y, 0) = 0\} = \left\{(x, y) : y = x^2 - \frac{x^3}{3}\right\}, \quad (7)$$

is called the *critical manifold*. We thus have two separate systems that combine to illustrate the global dynamics when $\epsilon = 0$ and $\lambda = 1$. The trajectories corresponding to the singular limits jump between the layer problem and reduced problem at two jump points, which will be understood as fold points later on. We shall restrict our attention to the jump at $(x_0^1, y_0^1) = (0, 0)$, the case for the point $(x_0^2, y_0^2) = (2, \frac{4}{3})$ is analogous. The aim is to fully understand the dynamics in a neighbourhood of these jump points for $\epsilon \ll 1$. Note that these points are equilibria of the reduced problem. Since the flow on S is determined by \dot{y} , it can be seen that since the sign of g is negative in the neighbourhood of the jump point $(0, 0)$, the slow flow on S is directed towards the jump points. It remains to show that the flow in these limiting cases persists under perturbation to $0 < \epsilon \ll 1$ and ascertain whether the behaviour is the same for all λ .

In order to understand the global dynamics of the full system when $\epsilon > 0$, we need to understand the dynamics in the singular system that is when $\epsilon \rightarrow 0$. We then need to conclude the persistence of the dynamics present in the singular limit for the full system. The standard theory and its limitations are discussed in the following section. The case when $\lambda \neq 1$ is discussed in Section 4, while the extension of the theory to three dimensions is discussed in Section 5 and 6.

2 Standard Theory for Fast-Slow Systems and Where It Fails

In this section the singular limit is analysed by considering the reduced dynamics of the fast-slow system when $\lambda = 1$ and identifying the points where the dynamics of the singular system, $\epsilon \rightarrow 0$, is not known. Moving on from that problem, the standard theory, called Geometric Singular Perturbation Theory, for concluding the persistence of the singular dynamics for the full system is introduced. Following this, the points where this theory does not hold are established.

2.1 Reduced Dynamics

In order to determine the reduced dynamics on the critical manifold S , we consider the reduced problem (6).

Rearranging the first equation, $f = 0$, of System 6, define the cubic $\phi(x) = x^2 - \frac{x^3}{3}$ can be defined. Then using the chain rule, we can express the change in x using the second equation of (6) as,

$$\phi_x(x)\dot{x} = g(x, \phi(x), 0). \quad (8)$$

Rearranging this gives an expression for the dynamics in x on S . The derivative with respect to x gives $\phi_x(x) = 2x - x^2$, therefore Equation 8 becomes,

$$\dot{x} = \frac{g(x, \phi(x), 0)}{\phi_x(x)} = \frac{x-1}{2x-x^2} = \frac{x-1}{x(2-x)}.$$

The reduced dynamics are singular at $x = 0$ and $x = 2$. Therefore, no conclusions about the dynamics of x can be made at the jump points in this system.

The dynamics in the layer problem (5) are simpler. In this system, the manifold S contains all the equilibria. Whatever the initial data, the position moves horizontally towards S at which point it stops. The issue of reconciling the reduced and layer problems is considered using geometric singular perturbation theory (GSPT) below, along with conditions for the persistence of the dynamics under perturbation in ϵ . However, this will not cover the singularities. The reasoning for this is given later on in this section. The blow up method is employed in Section 3 to address the singularities, as well as the problems encountered when trying to apply GSPT.

2.2 Geometric Singular Perturbation Theory

The main question GSPT aims to answer is the following: under what conditions can it be concluded that the dynamics on the critical manifold $S = S_0$, persist as an invariant manifold S_ϵ under a small perturbation $0 < \epsilon \ll 1$? The main contribution to GSPT comes from ? and his three theorems can be summed up in one, according to ?. However, before stating the theorem, some formal definitions are needed.

Definition 2.1. Normal Hyperbolicity (?)

A submanifold $M \subseteq S$ is called normally hyperbolic, if the Jacobian $\frac{\partial f}{\partial x}(x, y, \lambda, 0)$, where $(x, y) \in M$, has only eigenvalues with nonzero real part.

Moreover, the points $(x, y) \in M$, M normally hyperbolic, are hyperbolic equilibria of Equation 5 (?). A normally hyperbolic submanifold can be classified according to its stability property: If M only has eigenvalues with positive real part it is called repelling, otherwise eigenvalues with negative real part are called attracting and if M is neither attracting nor repelling it is called a saddle-type submanifold (?). Furthermore, stable and unstable manifolds can be defined as $W^s(M)$ and $W^u(M)$, corresponding to the eigenvalues with negative and positive real part, respectively. Now, with the following definition it is established which notion of distance is going to be employed throughout this analysis.

Definition 2.2. Hausdorff Distance (?)

The Hausdorff Distance of two nonempty sets $V, W \subset \mathbf{R}^n$, for some $n \in \mathbf{N}$ is defined as

$$d_H(V, W) = \max\{\sup_{v \in V} \inf_{w \in W} \|v - w\|, \sup_{w \in W} \inf_{v \in V} \|v - w\|\}.$$

Now combining the above we can state Fenichel's Theorem.

Theorem 2.3 (Fenichel's Theorem (?)

Suppose $M = M_0$ is a compact, normally hyperbolic submanifold (possibly with boundary) of the critical manifold S Equation 7 and that $f, g \in C^r, r < \infty$. Then for $\epsilon > 0$, sufficiently small, the following holds:

(F1) There exists a locally invariant manifold M_ϵ , diffeomorphic to M_0 . Local invariance means that M_ϵ can have boundaries through which trajectories enter or leave.

(F2) M_ϵ has a Hausdorff distance of $O(\epsilon)$ from M_0 .

(F3) The flow on M_ϵ converges to the slow flow as $\epsilon \rightarrow 0$.

(F4) M_ϵ is C^r -smooth.

(F5) M_ϵ is normally hyperbolic and has the same stability properties with respect to the fast variables as M_0 (attracting, repelling or saddle type).

(F6) M_ϵ is usually not unique. In regions that remain at a fixed distance from the boundary of M_ϵ , all manifolds satisfying (F1)-(F5) lie at a Hausdorff distance $O(e^{-K/\epsilon})$ from each other for some $K > 0$ with $K = O(1)$. The normally hyperbolic manifold M_0 has associated local stable and unstable manifolds

$$W^s(M_0) = \bigcup_{p \in M_0} W^s(p) \quad \text{and} \quad W^u(M_0) = \bigcup_{p \in M_0} W^u(p),$$

where $W^s(p)$ and $W^u(p)$ are the local stable and unstable manifolds of p as a hyperbolic equilibrium of the layer equations, respectively. These manifolds also persist for $\epsilon > 0$, sufficiently small. There exist locally stable and unstable manifolds $W^s(M_\epsilon)$ and $W^u(M_\epsilon)$, respectively, for which conclusions (F1)-(F6) hold if we replace M_ϵ and M_0 by $W^s(M_\epsilon)$ and $W^u(M_\epsilon)$ (or similarly by $W^u(M_\epsilon)$ and $W^s(M_\epsilon)$).

Fenichel's Theorem establishes that the submanifold, M_0 , of the critical manifold, S_0 , persists as slow manifold M_ϵ as $\epsilon > 0$, given it is compact and normally hyperbolic. The theorem furthermore establishes that the stable and unstable manifolds persist as well as the individual fibres, namely $W^s(p)$ and $W^u(p)$, that are associated to each base point $p \in M_0$. Therefore, under the assumptions of the theorem, the flow of the fast-slow system remains $O(\epsilon)$ close to the flow of the system in the singular limit $\epsilon \rightarrow 0$.

The importance of this result lies in the fact that the behaviour of the full system can be analysed by looking at the system in the singular limit instead. The main assumption that has to be satisfied in order to apply Theorem 2.3 is normal hyperbolicity. The points where this assumption fails is discussed in the following section.

2.3 Fold Points

One of the requirements of Fenichel's Theorem is normal hyperbolicity. However, fast-slow systems can display singular points where normal hyperbolicity is no longer given and therefore the conclusions of Theorem 2.3 no longer hold. These singularities are points where trajectories can jump between fast and slow flow. The singularities in the setting of fast-slow systems are points (x_0, y_0) on the critical manifold S_0 , for which the Jacobian has one or more eigenvalue with zero real part. Comparing this with Definition 2.1 shows that this is a negation of normal hyperbolicity. The simplest of those singularities are called fold points,

Definition 2.4. *Fold Point*

A fold point $(x_0, y_0) \in S_0$ is a point where the Jacobian $\frac{\partial f}{\partial x}(x_0, y_0, \lambda, 0)$ has only one eigenvalue with zero real part.

Moreover we say that the fold point is non-degenerate if it satisfies the non-degeneracy assumptions,

$$\begin{cases} \frac{\partial^2 f}{\partial x^2}(x_0, y_0, \lambda, 0) \neq 0, \\ \frac{\partial f}{\partial y}(x_0, y_0, \lambda, 0) \neq 0. \end{cases} \quad (9)$$

Furthermore, if (x_0, y_0) satisfies the transversality condition $g(x_0, y_0, \lambda, 0) \neq 0$, then it is called a generic fold point. For these generic folds the slow flow on S_ϵ near (x_0, y_0) has either positive or negative sign, implying that no equilibria of the slow flow are close to (x_0, y_0) . Therefore, for generic fold points no canards will be observed, which is a relevant observation for Section 4. First, we must find the fold points in the system.

2.4 The Van der Pol System: GSPT and Fold Points

The aim is to establish normal hyperbolicity of the reduced system in order to conclude that the manifold S_0 perturbs to a manifold S_ϵ . Since Theorem 2.3 concludes the persistence of the stable and unstable manifolds of S as well, we do not need to consider the normal hyperbolicity of the layer problem separately. In order to analyse the System (6), we note from the previous analysis that the expression for \dot{x} is dependent on the expression for \dot{y} . Therefore, it suffices to consider a one dimensional Jacobian,

$$J = \frac{\partial f}{\partial x} = 2x - x^2.$$

Then the eigenvalues corresponding to this are $\sigma = x(2 - x)$. These σ are zero at $x = 0$ and $x = 2$. At these points normal hyperbolicity is lost and Theorem 2.3 cannot be applied. Therefore, the critical manifold has to be divided as follows,

$$S^a = \left\{ (x, y) : y = x^2 - \frac{x^3}{3}, x < 0 \right\} \cup \left\{ (x, y) : y = x^2 - \frac{x^3}{3}, x > 2 \right\},$$

$$S^r = \left\{ (x, y) : y = x^2 - \frac{x^3}{3}, 0 < x < 2 \right\},$$

such that $S^a \cup S^r \cup \{0\} \cup \{2\} = S$. The manifolds S_0^a and S_0^r are normally hyperbolic everywhere and Fenichel's Theorem 2.3 can be applied in order to conclude the persistence of the manifold as slow manifolds S_ϵ^a and S_ϵ^r . At the points $x = 0$ and $x = 2$ the normal hyperbolicity is not given, since the eigenvalue associated to S is zero at these points. The next step of the analysis is to classify the nonhyperbolic points and conclude that they are generic folds. The points of interest are $(x_0^1, y_0^1) = (0, 0)$ and $(x_0^2, y_0^2) = \left(2, \frac{4}{3}\right)$. By Definition 2.4, there is only one eigenvalue with zero real part at (x_0, y_0) . These points are nondegenerate if the non-degeneracy assumptions (Equation 9) hold,

$$\frac{\partial^2 f}{\partial x^2}(x_0^1, y_0^1, 0) = 2 - 2x_0^1 = 2 \neq 0,$$

$$\frac{\partial f}{\partial y}(x_0^1, y_0^1, 0) = -1 \neq 0,$$

and equivalently for the other fold point

$$\frac{\partial^2 f}{\partial x^2}(x_0^2, y_0^2, 0) = -2x_0^2 = 4 \neq 0,$$

$$\frac{\partial f}{\partial y}(x_0^2, y_0^2, 0) = -1 \neq 0.$$

Therefore, the two fold points are non-degenerate. Furthermore, it can be checked if a fold point is generic. It then has to satisfy the transversality condition $g(x_0, y_0, 0) \neq 0$. The two fold points considered here are generic, since,

$$g(x_0^1, y_0^1, 0) = -1 \neq 0,$$

$$g(x_0^2, y_0^2, 0) = 1 \neq 0.$$

Note that systems containing non-generic folds or other types of singularities can display different behaviour.

In the analysis of the reduced system it became apparent that the fold points are singularities of the reduced flow on S_0 , and therefore the dynamics in the singular limit cannot be determined. Furthermore, Fenichel Theory does not apply at the folds because normal hyperbolicity breaks down at these points, as discussed above. Therefore, even if the dynamics around the folds in the singular limit were known, no conclusions could be drawn for the perturbed system with S_ϵ . Alternative methods have to be employed to describe the dynamics on the fold points in the singular limit and furthermore to be able to conclude the dynamics of the full system at the fold points from this analysis. The method considered for analysis is called the Blow-Up Method.

3 The Blow-Up Method

The canonical system Equation (4) is extended to three dimensions by considering $\epsilon' = 0$,

$$\begin{aligned} x' &= -y + x^2 + h(x), \\ y' &= \epsilon(x - 1), \\ \epsilon' &= 0. \end{aligned} \tag{10}$$

In order to apply the Blow-Up Method to the fold point at the origin, we focus on a neighbourhood U around the fold point $(0, 0)$. The neighbourhood U is small enough such that $g(x, y, \epsilon) \neq 0$ in U , and we can define sections in U as follows,

$$\begin{aligned} \Delta^{in} &= \{(x, \rho^2), x \in I\}, \\ \Delta^{out} &= \{(\rho, y), y \in \mathbf{R}\}, \end{aligned}$$

where $I \subset \mathbf{R}$. Now Δ^{in} is transverse to S^a , while Δ^{out} is transverse to the fast flow. This enables us to monitor the incoming trajectories from the attracting branch of S and the trajectories leaving U in the direction of the fast flow. Then a function $\pi : \Delta^{in} \rightarrow \Delta^{out}$ can be defined, called the transition map, which describes how the trajectories passing through Δ^{in} are mapped onto the outgoing flow in Δ^{out} . The following theorem describes the behaviour of the flow under π .

Theorem 3.1 (?)

Under the assumptions made in this section, there exists $\epsilon_0 > 0$ such that the following assertions hold for $\epsilon \in (0, \epsilon_0]$:

1. *The manifold S_ϵ^a passes through Δ^{out} at a point $(\rho, h(\epsilon))$, where $h(\epsilon) = O(\epsilon^{2/3})$.*
2. *The transition map π is a contraction with contraction rate $O(e^{-c/\epsilon})$, where c is a positive constant.*

This means that the trajectories that enter U through Δ^{in} , will be funnelled into a smaller section of Δ^{out} and therefore we are guaranteed to observe the trajectories that enter through Δ^{in} in Δ^{out} . Now we are in the position to describe the method of Blow-Up transformations in the neighbourhood U .

3.1 Coordinate Transformation and Charts

We first need to transform the Extended System (10) with respect to the time variable and the space variables. This coordinate transformation is called the Blow-Up transformation because the degenerate fold point $(0, 0)$ is regarded as a sphere of radius $r = 0$. By rescaling the space variables with respect to different weights of r ,

$$x = \bar{r}\bar{x} \tag{11a}$$

$$y = \bar{r}^2\bar{y} \tag{11b}$$

$$\epsilon = \bar{r}^3\bar{\epsilon}, \tag{11c}$$

we find that we are able to carry out further analysis, as will follow. Instead of analysing the sphere in spherical polar coordinates, which might seem the most obvious choice we use charts, described below (see ? for the construction of charts on a sphere). This method turns out to be a more natural choice for this problem and simplifies calculations. In terms of the blown up fold point, a sphere of radius

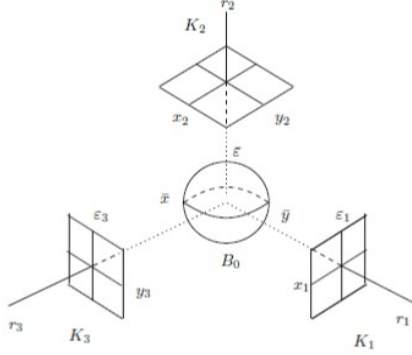


Figure 4: Three charts mapping different sections of our blow up (?).

zero denoted by B , charts are projections of regions of B onto a two dimensional plane. We introduce three charts K_1, K_2 , and K_3 . Chart K_2 is the two dimensional projection covering the upper half plane of B . However, as points on the equator of B are approached on K_1 , the point tends to infinity. These regions however, are of immense interest, since they are points of incoming and outgoing trajectories. As a consequence, charts K_1 and K_3 are introduced, covering the regions of interest on the equator of the fold point. The charts are defined by setting each of the variables of the extended system to 1 in turn, giving $\bar{y} = 1$, $\bar{\epsilon} = 1$, $\bar{x} = 1$. Substituting these into Equations (11a), (11b) and (11c) respectively gives,

$$x = r_1 x_1, \quad y = r_1^2, \quad \epsilon = r_1^3 \epsilon_1, \quad (12a)$$

$$x = r_2 x_2, \quad y = r_2^2 y_2, \quad \epsilon = r_2^3 \quad (12b)$$

$$x = r_3, \quad y = r_3^2 y_3, \quad \epsilon = r_3^3 \epsilon_3 \quad (12c)$$

where $(x_i, r_i, \epsilon_i) \in \mathbf{R}^3$ for $i = 1, 2, 3$, and the equations correspond to the charts in numerical order (?). With this setup, we can consider the dynamics on the individual charts, and then join the gathered information into a global view on the dynamics in U . We start with K_2 , because it holds the most information and the flow is analysed more readily than in the other two charts. The remaining question is how the transition between the three charts and the connection to the global dynamics is made after finishing the individual analysis. This is done via a coordinate change, derived by using Equations (12) and (11), and the results are summarised in the following lemma:

Lemma 3.2

Let κ_{12} denote the change of coordinates from K_1 to K_2 . Then κ_{12} is given by

$$x_2 = x_1 \epsilon_1^{-1/3}, \quad y_2 = \epsilon_1^{-2/3}, \quad r_2 = r_1 \epsilon_1^{1/3},$$

for $\epsilon_1 > 0$, and κ_{12}^{-1} is given by

$$x_1 = x_2 y_2^{-1/2}, r_1 = r_2 y_2^{1/2}, \epsilon_1 = y_2^{-3/2},$$

for $y_2 > 0$. Let κ_{23} denote the change of coordinates from K_2 to K_3 . Then κ_{23} is given by

$$r_3 = r_2 x_2, y_3 = y_2 x_2^{-2}, \epsilon_3 = x_2^{-3},$$

for $x_2 > 0$, and κ_{23}^{-1} is given by

$$x_2 = \epsilon_3^{-1/3}, y_2 = y_3 \epsilon_3^{-2/3}, r_2 = r_3 \epsilon_3^{1/3},$$

for $\epsilon_3 > 0$.

Furthermore, transition maps $\Pi_i, i \in 1, 2, 3$ are defined in each section, describing how the trajectories coming in and out of each chart. These are combined in the final part of this section to give the proof of Theorem 3.1, and to relate the results of the Blow Up Method back to the original transition map π .

3.2 Dynamics in K_2

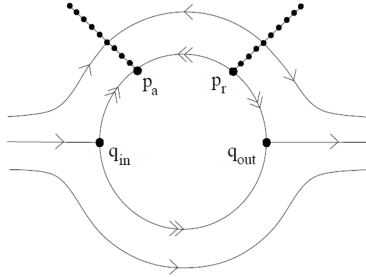


Figure 5: Phase portrait for chart 2 (?).

To be able to consider chart K_2 , the transformation presented in Equation (12b) is applied to the Extended System (10). Furthermore, a time rescaling ($t_2 = r_2 t$) is applied to desingularise the system. This results in,

$$\begin{aligned} \frac{d}{dt}(r_2 x_2) &= r_2^2 \frac{dx_2}{dt} = -y_2 + x_2^2 - \frac{x_2^3 r_2}{3}, \\ r_2^3 y'_2 &= r_2^3 (-1 + r_2 x), \\ r'_2 &= 0, \end{aligned} \tag{13}$$

noting that $\frac{dr}{dt_2} = \frac{dt}{dt_2} \frac{dr}{dt} = \frac{1}{r_2} \frac{dr_2}{dt}$. Now dividing through by r_2^2 and r_2^3 respectively for each equation and grouping $O(r_2)$ terms we get,

$$\begin{aligned} x'_2 &= x_2^2 - y_2 + O(r_2), \\ y'_2 &= -1 + O(r_2), \\ r'_2 &= 0. \end{aligned} \tag{14}$$

Then, considering $r_2 = 0$ and neglecting the $O(r_2)$ terms results in,

$$\begin{aligned} x'_2 &= x_2^2 - y_2, \\ y'_2 &= -1, \end{aligned} \tag{15}$$

which are the well known Riccati equations – see ?. Some known results about the Riccati equations can be summarised as follows:

Proposition 3.3 (?)

The Riccati equation (15) has the following properties:

1. *Every orbit has a horizontal asymptote $y = y_r$, where y_r depends on the orbit such that $x \rightarrow \infty$ as y approaches y_r from above.*
2. *There exists a unique orbit γ_2 , which can be parameterised as $(x, s(x))$, $x \in \mathbf{R}$ and is asymptotic to the left branch of the parabola $x^2 - y = 0$, for $x \rightarrow -\infty$. The orbit γ_2 has a horizontal asymptote $y = -\Omega_0 < 0$, such that $x \rightarrow \infty$ as y approaches $-\Omega_0$ from above.*
3. *The function $s(x)$ has the asymptotic expansions*

$$\begin{aligned} s(x) &= x^2 + \frac{1}{2x} + O\left(\frac{1}{x^4}\right), x \rightarrow -\infty, \\ s(x) &= -\Omega_0 + \frac{1}{x} + O\left(\frac{1}{x^3}\right), x \rightarrow \infty. \end{aligned}$$

4. *All orbits to the right of γ_2 are backward asymptotic to the right branch of the parabola $x^2 - y = 0$.*
5. *All orbits to the left of γ_2 have a horizontal asymptote $y = y_l > y_r$, where y_l depends on the orbit, such that $x \rightarrow -\infty$ as y approaches y_l from below.*

The solutions to the Riccati equations, described in Proposition 3.3, are displayed in Figure 6. Note that the equation $x^2 - y = 0$ is locally the critical manifold S close to the fold point. The orbit γ_2 corresponds to the global trajectory γ , of the full system, which is the candidate trajectory connecting the slow flow on S^a entering U through p_a to the fast fibres, exiting U through q_{out} – described by Figure 6.

This leads to the conclusion that if we can connect γ_2 to p_a through K_1 and to q_{out} through K_3 , the global γ can be constructed using Lemma 3.2. This motivates the analysis of K_1 and K_3 . In order to connect the dynamics on K_2 to that on the other charts, we need to define local inflow and outflow sections, similar to Δ^{in} and Δ^{out} in the full system. Then we can follow trajectories that get mapped by Π_2 , again analogous to π in the full system, from a section Σ_2^{in} to Σ_2^{out} . The sections are defined as follows. For $\delta > 0$, we have,

$$\begin{aligned} \Sigma_2^{in} &= \{(x_2, y_2, r_2) : y_2 = \delta^{-2/3}\}, \\ \Sigma_2^{out} &= \{(x_2, y_2, r_2) : x_2 = \delta^{-1/3}\}. \end{aligned}$$

The transition map Π_2 can then be defined and the results are summarised as follows:

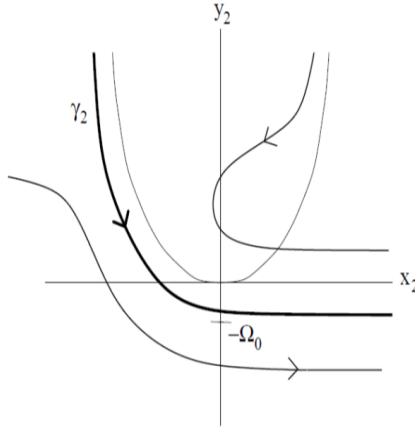


Figure 6: Riccati solution for chart 2 (?).

Proposition 3.4 (?)

The transition map Π_2 has the following properties:

1. $\Pi_2(q_0) = (\delta^{-1/3}, -\Omega_0 + \delta^{1/3} + O(\delta), 0)$
2. A neighbourhood of q_0 is mapped diffeomorphically onto a neighbourhood of $\Pi_2(q_0)$.

This is sufficient information to now consider the dynamics on K_1 .

3.3 Dynamics in K_1

The coordinate transformation (12a) is applied to the extended system (10),

$$\begin{aligned} \frac{d(r_1 x_1)}{dt_1} \frac{dt_1}{dt} &= -r_1^2 + r_1^2 x_1^2 - \frac{1}{3} r_1^3 x_1^3, \\ \frac{dr_1^2}{dt_1} \frac{dt_1}{dt} &= 2r_1^2 r_1' = r_1^3 \epsilon_1 (-1 + r_1 x_1), \\ \frac{d(r_1^3 \epsilon_1)}{dt_1} \frac{dt_1}{dt} &= (3r_1^2 \epsilon_1 + r_1^3 \epsilon_1') r_1 = 0. \end{aligned}$$

Dividing through by $\frac{dt_1}{dt} = r_1$ and replacing the expressions for ϵ_1' and r_1' , results in the full system in terms of K_1 . Note that the equation for ϵ' is found by rearranging the third equation above, such that

$$\begin{aligned} x_1' &= -1 + x_1^2 + \frac{1}{2} x_1 \epsilon_1 + \left(-\frac{1}{2} \epsilon_1 x_1^2 r_1 - \frac{1}{3} x_1^3 \right), \\ r_1' &= \frac{1}{2} r_1 \epsilon_1 (-1 + r_1 x_1), \\ \epsilon_1' &= \frac{3}{2} \epsilon_1^2 (1 - r_1 x_1), \end{aligned}$$

and grouping terms in r_1 results in the standard form,

$$\begin{aligned} x'_1 &= -1 + x^2 + \frac{1}{2}x_1\epsilon_1 + O(r_1), \\ r'_1 &= \frac{1}{2}r_1\epsilon_1(-1 + O(r_1)), \\ \epsilon'_1 &= \frac{3}{2}\epsilon_1^2(1 - O(r_1)). \end{aligned} \quad (16)$$

The system (16) has two invariant planes, that are somewhat equivalent to the notion of a nullcline. This tell us that the rate of change for our confidantes, r_1 and ϵ_1 is constant for $r_1 = 0$ and $\epsilon_1 = 0$. If we substitute $r_1 = 0$ or $\epsilon_1 = 0$ into (16), the r_1 or ϵ_1 equation respectively, are both zero, and there is only a two dimensional system left to consider. These two subspaces of (16) will be analysed below. Furthermore, the subspace where $r_1 = 0$ and $\epsilon_1 = 0$, is one dimensional, an invariant line, where the subspaces $r_1 = 0$ and $\epsilon_1 = 0$ cross. The following analysis is displayed in Figure 7, illustrating the dynamics on K_1 .

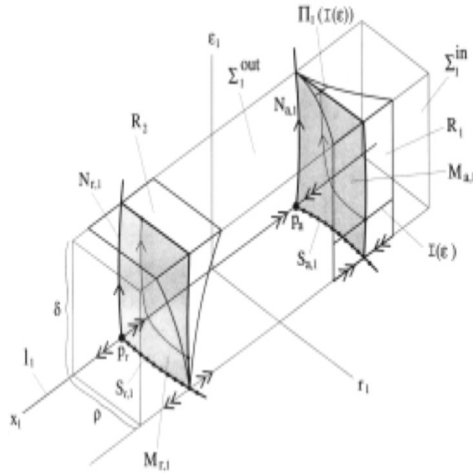


Figure 7: Dynamics in chart 1 (?)

The invariant line satisfying $r_1 = 0$ and $\epsilon_1 = 0$ is given by $l_1 = -1 + x^2$. From this it is easily deduced that the two equilibrium points are where $l_1 = 0$, which is at $x = \pm 1$. Therefore, the points p_a and p_r are defined as $p_a = (-1, 0, 0)$ and $p_r = (1, 0, 0)$. The flow on l_1 is attracted to p^a and repelled by p^r , which is easily observed from the form l_1 takes or from a formal stability analysis of the one dimensional system. The eigenvalues of l_1 are found by considering $l'_1 - \sigma = 2x - \sigma = 0$ which gives that $\sigma = \pm 2$ at the respective equilibria. Then we expect the behaviour of the flow on the two invariant planes to be influenced by the two equilibria and the dynamics on l_1 . Consider the plane $\epsilon_1 = 0$. The System (16) becomes

$$\begin{aligned} x'_1 &= -1 + x_1^2 - \left(\frac{1}{3} r_1 x_1^3 \right), \\ r'_1 &= 0. \end{aligned} \tag{17}$$

This system has equilibria at $x = \pm 1$, for $r_1 = 0$, as before. However, for each constant value of r_1 , we get a different equilibrium of the system (17). This forms a curve of equilibria, which can be recognised as S_1^a connected to p_a and S_1^r connected to p_r , of the critical manifold transformed into K_1 - this follows from the Implicit Function Theorem, see Figure 5. The additional eigenvalue, corresponding to the r_1 equation, is $\lambda = 0$. However, at each of the equilibria of this system, and specifically at p_a and p_r we have normal hyperbolicity, due to the coordinate transformation in K_1 . Next we consider the dynamics on the invariant plane $r_1 = 0$. The System (16) becomes,

$$\begin{aligned} x'_1 &= -1 + x^2 + \frac{1}{2} x_1 \epsilon_1, \\ \epsilon'_1 &= \frac{3}{2} \epsilon_1^2. \end{aligned} \tag{18}$$

Again, $x = \pm 1$ are equilibria of the system, and an additional zero eigenvalue is gained due to the ϵ equation. It can be concluded that one dimensional centre manifolds exist, called $N_{a,1}$ and $N_{r,1}$, that are invariant, but not manifolds of equilibria like S^a and S^r in the $\epsilon = 0$ plane. The dynamics on these manifolds are determined mainly by the value of ϵ , since the change in the ϵ direction is much stronger than the change in the x direction. Therefore, on $N_{a,1}$ and $N_{r,1}$ the flow moves in the ϵ direction with increasing epsilon. In order to draw conclusions on the persistence of the dynamics in the full system, sections in the space are defined to monitor incoming and outgoing trajectories. Firstly, define $D_1 := \{(x_1, y_1, \epsilon_1) : x_1 \in \mathbf{R}, 0 \leq r_1 \leq \rho, 0 \leq \epsilon_1 \leq \delta\}$. Then the relevant sections for the candidate trajectory γ are,

$$\begin{aligned} \Sigma_1^{in} &:= \{(x_1, r_1, \epsilon_1) \in D_1 : r_1 = \rho\}, \\ \Sigma_1^{out} &:= \{(x_1, r_1, \epsilon_1) \in D_1 : \epsilon_1 = \delta\}. \end{aligned}$$

Note that $\Sigma_1^{in} = \Delta^{in}$ and $\Sigma_1^{out} = \Sigma_2^{in}$. The aim is to find the connection between p_a and γ_2 in K_2 . In order to establish this connection, the trajectory γ_2 has to be mapped onto K_1 using Lemma 3.2. Recall from Section 3.2 that the form of the candidate trajectory is of the form $(x_2, s(x_2))$. Therefore,

the trajectory γ_1 satisfies:

$$(x_1, 0, \epsilon_1) = \left(x_2 \left(x_2^2 + \frac{1}{2x_2} + O\left(\frac{1}{x_2^4}\right) \right)^{-1/2}, 0, \left(x_2^2 + \frac{1}{2x_2} + O\left(\frac{1}{x_2^4}\right) \right)^{-3/2} \right).$$

Note that $s(x_2)$ as $x_2 \rightarrow -\infty$ is employed, since we consider the left continuation of γ_2 . Furthermore, as is intuitively clear from Figure 6, and can be shown by analysing the form of γ_1 , the trajectory γ_1 converges to p_a in backward time, as expected. This establishes the link between the slow flow on S^a and the flow on K_2 , if we consider the following proposition, which sums up the findings in K_1 and employs center manifold theory in order to establish persistence in the full system.

Proposition 3.5 (?)

For ρ, δ sufficiently small the following assertions hold for the system 16:

1. There exists an attracting two-dimensional C^k -center manifold $M_{a,1}$ at p_a which contains the line of equilibria S_1^a and the center manifold $N_{a,1}$. In D_1 the manifold $M_{a,1}$ is given as a graph $x_1 = h_a(r_1, \epsilon_1)$. The branch of $N_{a,1}$ in $r_1 = 0, \epsilon_1 > 0$ is unique.
2. There exists a repelling two-dimensional C^k -center manifold $M_{r,1}$ at p_r which contains the line of equilibria S_1^r and the center manifold $N_{r,1}$. In D_1 the manifold $M_{r,1}$ is given as a graph $x_1 = h_r(r_1, \epsilon_1)$. The branch of $N_{r,1}$ in $r_1 = 0, \epsilon_1 > 0$ is not unique.
3. There exists a stable invariant foliation F^s with base $M_{a,1}$ and one-dimensional fibres. For any $c > -2$ there exists a choice of positive ρ and δ such that the contraction along F^s during a time interval $[0, T]$ is stronger than e^{cT} .
4. There exists an unstable invariant foliation F^u with base $M_{r,1}$ and one-dimensional fibres. For any $c > -2$ there exists a choice of positive ρ and δ such that the expansion along F^u during a time interval $[0, T]$ is stronger than e^{cT} .
5. The unique branch $N_{a,1}$ in $r_1 = 0, \epsilon_1 > 0$ is equal to $\gamma_1 := \kappa_{12}^{-1}(\gamma_2)$ wherever $\kappa_{12}^{-1}(\gamma_2)$ is defined, i.e. along the part of γ_2 corresponding to $y_2 > 0$.

In order to find the lower bound on the contraction rate along F^s , the transition time T has to be found, that is the time the trajectory takes to travel from a point $p = (x_1, \rho, \epsilon_1) \in \Sigma_1^{in}$ to a point in $\Pi_1(p) = (x_1, r_1, \delta) \in \Sigma_1^{out}$. This is done by integrating the ϵ equation of system (16), which is a separable ODE with respect to t_1 . This then results in,

$$T = \frac{2}{3} \left(\frac{1}{\epsilon_1} - \frac{1}{\delta} \right) (1 + O(\rho)),$$

where $r_1 = \rho \in p$. Therefore, a transition map $\Pi_1 : \Sigma_1^{in} \rightarrow \Sigma_1^{out}$ can be defined for small enough parameter values of ρ, δ, β_1 . We are interested specifically in the transition around the center manifolds $M_{a,1}$ and $M_{r,1}$. The following subsections of Σ_1^{in} and Σ_1^{out} can be defined. Let $R_1 = \{(x_1, \rho, \epsilon_1) : |1 + x_1| \leq \beta_1\}$, a rectangle in the intersection of the manifolds $M_{a,1}$ and Σ_1^{in} , and $R_2 = \{(x_1, r_1, \delta) : |1 + x_1| \leq \beta_1\}$,

$|1 - x_1| \leq \beta_1\}$, a rectangle in the intersection of the manifolds $M_{r,1}$ and Σ_1^{out} , with $\beta_1 > 0$ sufficiently small. Furthermore, we can define line segments in these rectangles as $I_a(\bar{\epsilon}) \subset R_1$ and $I_r(\bar{r}) \subset R_2$, where $0 \leq \bar{\epsilon} \leq \delta$ and $0 \leq \bar{r} \leq \rho$. Then for any $\bar{\epsilon}$, Π_1 maps the trajectory on a smaller region $\Pi_1 I_a(\bar{\epsilon}) \in \Sigma_1^{out}$. This is called a contraction of the trajectories. Considering Theorem 3.1, which states the dependence of the contraction rate on ϵ , the bounds on the contraction rate can be related to ϵ , the parameter of the original system. Then using the K_1 rescaling of $\epsilon = \epsilon_1 r_1^3$, see Equation 12a, the contraction rate for $\Pi_1|I_r(\bar{r})$ is found by replacing ϵ_1 by $\frac{\delta r^3}{\rho^3}$. Visual understanding of this analysis can be gained by considering Figure 7. The following proposition summarises the the findings for Π_1 :

Proposition 3.6 (?)

For ρ, δ and β_1 sufficiently small, the transition map $\Pi_1 : \Sigma_1^{in} \rightarrow \Sigma_1^{out}$ defined by the flow of system 16 has the following properties:

1. $\Pi_1(R_1)$ is a wedge- like region in Σ_1^{out} . $\Pi_1^{-1}(R_2)$ is a wedge- like region in Σ_1^{in} .
2. More precisely, for fixed $c < 2$, there exists a constant K depending on the constants c, ρ, δ and β_1 such that:
 - (a) for $\bar{\epsilon} \in (0, \delta]$ the map $\Pi_1|I_a(\bar{\epsilon})$ is a contraction with contraction rate bounded by $Ke^{-\frac{2c}{3}(\frac{1}{\bar{\epsilon}} - \frac{1}{\delta})}$.
 - (b) for $\bar{r} \in (0, \rho]$ the map $\Pi_1|I_r(\bar{r})$ is a contraction with cocontraction rate bounded by $Ke^{-\frac{2c}{3}\left(\frac{\rho^3}{r_1^3 \delta} - \frac{1}{\delta}\right)}$.

3.4 Dynamics in K_3

Next we study the behaviou of K_3 . This chart covers the trajectory as it leaves the fold point at q_{out} . The other charts could not do this as q_{out} is close to infinity in both K_1 and K_3 (cf. Figure 4). Similarly to K_1 and K_2 , the system can be analysed using the blow-up transformation (12c),

$$\frac{dr_3}{dt_3} = r_3 F(r_3, y_3, \epsilon_3), \quad (19a)$$

$$\frac{dy_3}{dt_3} = \epsilon_3(r_3 - 1) - 2y_3 F(r_3, y_3, \epsilon_3), \quad (19b)$$

$$\frac{d\epsilon_3}{dt_3} = -3\epsilon_3 F(r_3, y_3, \epsilon_3), \quad (19c)$$

where $F(r_3, y_3, \epsilon_3) = (1 - y_3 - \frac{r_3}{3})$. Note that as ϵ_3 and r_3 appear as a factor in their respective derivatives, the planes $\epsilon_3 = 0$ and $r_3 = 0$ are invariant and, by extension, so is the y_3 axis. The aim is to continue the special trajectory found in the other two charts and to find the transition map in and out of this chart. We will then be able to construct a phase portrait for the whole space by combining the dynamics in each chart. Linearising the system about $(0, 0, 0) = q_{out}$ gives,

$$\begin{pmatrix} \dot{r}_3 \\ \dot{y}_3 \\ \dot{\epsilon}_3 \end{pmatrix} = \begin{pmatrix} 1 & 0 & 0 \\ 0 & -2 & -1 \\ 0 & 0 & -3 \end{pmatrix} \begin{pmatrix} r_3 \\ y_3 \\ \epsilon_3 \end{pmatrix}.$$

As the matrix is upper triangular, its eigenvalues are trivially $\{1, -2, -3\}$ with corresponding eigenvectors $\{(1, 0, 0), (0, 1, 0), (0, 1, 1)\}$. This presents an issue as there is additive resonance that is $\lambda_2 - (\lambda_1 + \lambda_3) = 0$. This means the Poincaré-Dulac theorem does not hold and the vector field is not linearisable, there is no smooth transformation between the nonlinear and linear flow. Despite this, progress can still be made as the form of the equations allow a near identity transformation and yields the lowest order approximation to the flow. The special orbit, γ_2 , can be mapped into this chart using the change of coordinates κ_{23} of Equation 3.2,

$$\gamma_3 = \kappa_{23}(\gamma_2).$$

In fact, γ_3 lies in the plane $r_3 = 0$ and converges to q_{out} as $\epsilon \rightarrow 0$. To find the flow in a neighbourhood of q_{out} we use sections similar to those introduced in K_2 ,

$$\begin{aligned}\Sigma_3^{in} &= \{(r_3, y_3, \epsilon_3) : r_3 \in [0, \rho], y_3 \in [-\beta_3, \beta_3], \epsilon_3 = \delta\}, \\ \Sigma_3^{out} &= \{(r_3, y_3, \epsilon_3) : r_3 = \rho, y_3 \in [-\beta_3, \beta_3], \epsilon_3 \in [0, \delta]\}.\end{aligned}$$

We now wish to find the transition map Π_3 between these two charts. That is, given that the trajectory enters somewhere in Σ_3^{in} , how will it behave until it reaches Σ_3^{out} ? To do this, the system 19 will be studied after some simplification. The system is in fact equivalent to the Riccati equation. Observe that $F(r_3, y_3, \epsilon_3)|_{q_{out}} = 1 - y_3 + O(r_3)|_{q_{out}} \approx 1$. Thus dividing (19) through by F yields,

$$\dot{r}_3 = r_3, \tag{20a}$$

$$\dot{y}_3 = -2y_3 - \frac{\epsilon_3}{1 - y_3} + r_3\epsilon_3 G(r_3, y_3, \epsilon_3), \tag{20b}$$

$$\dot{\epsilon}_3 = -3\epsilon_3. \tag{20c}$$

In the invariant plane $r_3 = 0$, the system becomes the Riccati equation (compare with Equation (15)) transformed into the chart K_3 and with a rescaling of time,

$$\begin{aligned}y'_3 &= -2y_3 - \frac{\epsilon_3}{1 - y_3}, \\ \epsilon'_3 &= -3\epsilon_3.\end{aligned}$$

This system has eigenvalues $\{-2, -3\}$ and the issue of additive resonance has been avoided so we are able to linearise the system using a near-identity transformation. This transformation allows the elimination of awkward higher order terms (in this case, $\frac{1}{1-y_3}$). Let

$$y_3 = \psi(\tilde{y}_3, \epsilon_3) = \tilde{y}_3 + O(\tilde{y}_3\epsilon_3).$$

Let $\tilde{\psi}$ denote the inverse transformation and both be C^k functions. The system (20) can now be linearised and the following proposition gives the transition map.

Proposition 3.7 (?)

The transition map Π_3 for the transformed K_3 system (19) is

$$\Pi_3(r_3, y_3, \delta) = \begin{pmatrix} \rho \\ \Pi_{32}(r_3, y_3, \delta) \\ \left(\frac{r_3}{\rho}\right)^3 \delta \end{pmatrix},$$

where

$$\Pi_{32}(r_3, y_3, \delta) = (\bar{\psi}(y_3, \delta) - \delta) \left(\frac{r_3}{\rho}\right)^2 + O(r_3^3 \ln r_3).$$

Proof. We will use the near-identity transformation to find the passage time T and thus the values of r_3, y_3, ϵ_3 at this time. For brevity, the subscripts will be omitted for the remainder of this proof. Under the near-identity transformation, system (20) becomes,

$$\dot{r} = r, \tag{21a}$$

$$\dot{\tilde{y}} = -2\tilde{y} + \epsilon + r\epsilon H(r, \tilde{y}, \epsilon), \tag{21b}$$

$$\dot{\epsilon} = -3\epsilon. \tag{21c}$$

Let the subscript i denote the value of a variable at its entry into the chart, and likewise o for out. Then $(r_i, y_i, \epsilon_i) \in \Sigma^{in}$, and $(r_o, y_o, \epsilon_o) \in \Sigma^{out}$. Thus

$$\begin{aligned} r(0) &= r_i, & r(T) &= r_o = \rho, \\ y(0) &= y_i, & y(T) &= y_o, \\ \epsilon(0) &= \epsilon_i = \delta, & \epsilon(T) &= \epsilon_o. \end{aligned}$$

We wish to construct an equation for the out variables $(T, \tilde{y}_o, \epsilon_o)$ in terms of the in variables (r_i, \tilde{y}_i) , that is the transition map. The r and ϵ equations are easily solved,

$$r = r_i e^t, \tag{22}$$

$$\epsilon = \delta e^{-3t}. \tag{23}$$

Then using $r(T) = \rho$,

$$r(T) = \rho = r_i e^{-t} \implies T = \ln\left(\frac{\rho}{r_i}\right).$$

For the equation in y , a little more work is required. We introduce a new coordinate z as follows, $\tilde{y} = e^{-2t}(\tilde{y}_i - \delta + z) + \delta e^{-3t}$. Upon first sight, this seems unlikely to be of any use. However, it turns out that this transformation is ideal as it allows many terms to be removed. First rearrange for z and differentiate with respect to t ,

$$\begin{aligned} z &= e^{2t}(\tilde{y} - \delta e^{-3t}) - \tilde{y}_i + \delta, \\ \frac{dz}{dt} &= 2e^{2t}\tilde{y} + e^{2t}\dot{\tilde{y}} + \delta e^{-t}. \end{aligned}$$

Substitute $\dot{\tilde{y}}$ from Equation (21b) and cancel terms,

$$\begin{aligned} &= e^{2t}(-\epsilon + r\epsilon H(r, \tilde{y}, \epsilon)) + \delta e^{-t}, \\ &= -\epsilon e^{2t} + e^{2t}r\epsilon H(r, \tilde{y}, \epsilon) + \delta e^{-t}, \\ &= e^{2t}r\epsilon H(r, \tilde{y}, \epsilon). \end{aligned}$$

This final equality follows from the explicit solutions in r and ϵ above. These equations also show that $r\epsilon e^{2t} = r_i \delta e^{-2t} e^{2t}$. Finally,

$$\dot{z} = r_i H^z(r_i, \tilde{y}_i, t),$$

where H^z is the same as H but under the transformation from z , i.e. $H^z(r_i, \tilde{y}_i, t) = \delta H(r_i e^t, e^{-2t}(\tilde{y}_i - \delta + z) + \delta e^{-3t}, \delta e^{-3t})$. This has not affected the expression for the passage time T . Hence $z(T) = r_i O(T) = O(r_i \ln(\frac{\rho}{r_i}))$. Using the initial definition of z , we recover an expression for $\tilde{y}(T)$.

$$\begin{aligned} \tilde{y}(T) &= e^{-2T} \left(\tilde{y}_i - \delta + O \left(r_i \ln \left(\frac{\rho}{r_i} \right) \right) \right) + \delta e^{-3T}, \\ &= (\tilde{y}_i - \delta) e^{-2 \ln \frac{\rho}{r_i}} + e^{-2 \ln \frac{\rho}{r_i}} O \left(r_i \ln \frac{\rho}{r_i} \right) + \delta \frac{r_i^3}{\rho^3}, \\ &= (\tilde{y}_i - \delta) \frac{r_i^2}{\rho^2} + O \left(\frac{r_i^3}{\rho^2} \ln \frac{\rho}{r_i} \right). \end{aligned}$$

We now have an expression for each of the out variables in terms of the initial conditions, albeit under a near-identity transformation. All that remains is to undo this transformation using the inverse map $\tilde{\psi}$,

$$\begin{aligned} \Pi_{32}(r_3, y_3, \delta) &= \psi \left(\left(\tilde{\psi}(y_3, \delta) - \delta \right) \left(\frac{r_3}{\rho} \right)^2 + O(r_3^3 \ln r_3), \left(\frac{r_3}{\rho} \right)^3 \delta \right), \\ &= (\tilde{\psi}(y_3, \delta) - \delta) \left(\frac{r_3}{\rho} \right)^2 + O(r_3^3 \ln r_3). \end{aligned}$$

The result then follows by expressing r_3 and ϵ_3 as functions of the out variables, that is $r_3(T) = \rho$ and $\epsilon_3(T) = \delta \left(\frac{r_3}{\rho} \right)^3$. ■

3.5 The Full Solution

The analysis of the three charts, discussed in the Sections 3.2-3.4, provided a description of the dynamics on each of the charts, as well as theory to conclude the persistence of the dynamics in the full system. The special trajectory γ has been traced through all charts and in chart 1 it has been linked to the slow flow of S^a , while in chart 3 the connection to the fast flow has been made. Therefore, the fold point is indeed a jump point, or transition point, which connects the slow and fast dynamic. These transition points can also be seen in the case of singular canards, which are treated in the following section. The remaining issue is the transition of this special trajectory through the charts in order to

have a solution of the full system. This is equivalent to finding the transition map π from Theorem 3.1. Let $\Pi : \Sigma_1^{in} \rightarrow \Sigma_3^{out}$ be the full transition map of the Blow-Up transformation. Then it satisfies

$$\Pi := \Pi_3 \circ \kappa_{23} \circ \Pi_2 \circ \kappa_{12} \circ \Pi_1,$$

where κ is the change of coordinates defined in Lemma 3.2 and Π_1, Π_2, Π_3 are the transition maps in each chart. Finally, reversing the blow up transformation gives the full transition map π and therefore there exists a trajectory γ in the blown down vector field connecting slow and fast flow. With this analysis at hand we are now able to describe the full dynamics of the Van der Pol system when $\epsilon > 0$ by analysing the singular limit $\epsilon \rightarrow 0$. The full result is visualised in Figure 8.

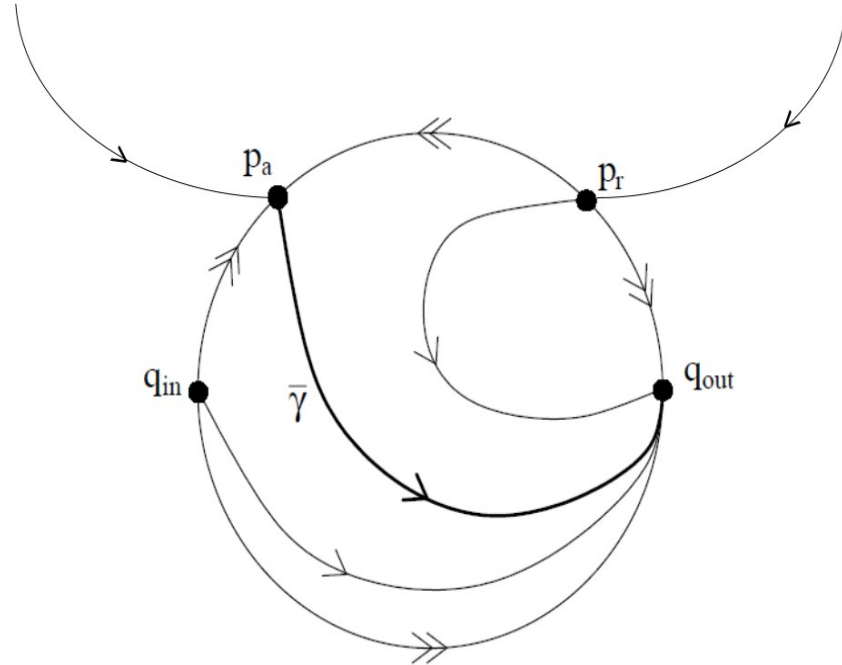


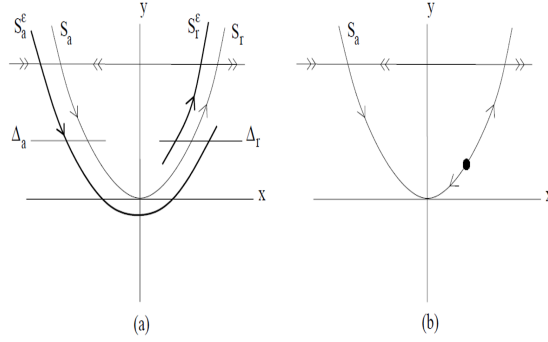
Figure 8: The full solution associated with the flow on the fold point.

4 Canards in Two Dimensions

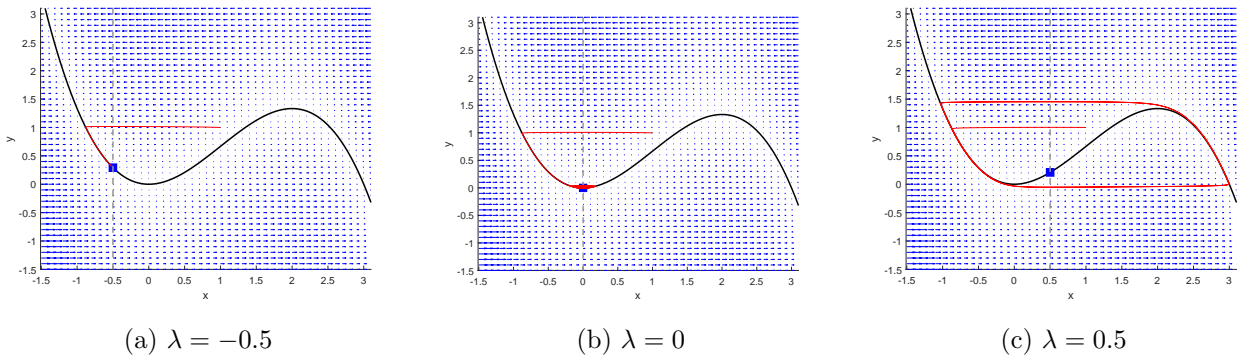
We have now found the global dynamics for the Van der Pol system with $\epsilon > 0$ for $\lambda = 1$. It is now of interest to investigate whether changing λ causes a qualitative change in the dynamics of the Van der Pol system. Consider the Van der Pol System with $\lambda \neq 1$,

$$\begin{aligned} x' &= -y + x^2 - \frac{x^3}{3}, \\ y' &= \epsilon(x - \lambda). \end{aligned} \tag{24}$$

Since the nullcline $\dot{y} = 0 \Rightarrow x = \lambda$ depends on λ , varying λ corresponds to a shift of the equilibrium along the S shaped curve. Numerical experiments show that solutions to the full system are either


 Figure 9: The reduced flow where a) $\lambda = 0$ and b) $\lambda > 0$.

relaxation oscillations when the equilibrium lies between the fold points. That is, when it is on the repelling branch. When the equilibrium lies on the attracting branch, all trajectories converge to this point (when $\lambda > 2$ or $\lambda < 0$). Naturally, there must be a change of stability when $\lambda = 0$ and when $\lambda = 2$. In this section we aim to explain the nature of this shift in stability and its effect on the global dynamics rigorously. Figure 10 gives an initial idea of the behaviour when λ is close to 0. We will restrict attention to this point as the case for $\lambda = 2$ is entirely analogous. Trajectories that pass close to this fold point are called canards, more rigorous definitions are given below.


 Figure 10: Example trajectories for varying λ . Note the small amplitude oscillations when $\lambda = 0$.

Definition 4.1 (Canard (?)). *A trajectory of a fast-slow system is called a canard if it stays within $O(\epsilon)$ close to the repelling branch S^r of the slow manifold S , for some time of $O(1)$ on the slow time scale $\tau = \epsilon t$.*

Furthermore, the following definition turns out to be useful as well:

Definition 4.2 (Maximal Canard (?)). *The trajectory passing through the intersection of S^a and S^r is called a maximal canard.*

Definition 4.3 (Singular Canard (?)). *Trajectories of the slow flow lying in the attracting and repelling parts of the critical manifold are called singular canards.*

We expect singular canards in the reduced system to perturb to maximal canards in the full system. We follow a similar process as to when $\lambda = 1$. First, some nondegeneracy conditions are required. These are, as before, applied at the fold point $(0, 0)$. Note that in contrast to the nondegeneracy conditions in (9), the transversality condition $g(0, 0, 0) \neq 0$ is not satisfied. Therefore higher order conditions on g have to be employed, in particular these are nonzero derivatives of g with respect to x and λ . The fact that $g_x(0, 0, 0) \neq 0$ guarantees the existence of transversal intersection of the two nullclines, which is crucial in order to conclude persistence of the dynamics. The constraint on the derivative of g with respect to λ ensures that the nullcline passes through the fold point with nonzero speed (?). The nondegeneracy and transversality conditions for the canard case are (?),

$$f(0, 0, 0, 0) = 0, \quad \frac{\partial}{\partial x} f(0, 0, 0, 0) = 0, \quad g(0, 0, 0, 0) = 0, \quad (25)$$

$$\begin{aligned} \frac{\partial^2}{\partial x^2} f(0, 0, 0, 0) &\neq 0, \quad \frac{\partial}{\partial y} f(0, 0, 0, 0) \neq 0, \\ \frac{\partial}{\partial x} g(0, 0, 0, 0) &\neq 0, \quad \frac{\partial}{\partial \lambda} g(0, 0, 0, 0) \neq 0. \end{aligned} \quad (26)$$

Now that these conditions have been defined we can consider, equivalent to the argument in Section 3, the extended Van der Pol system,

$$\begin{aligned} x' &= -y + x^2 - \frac{x^3}{3}, \\ y' &= \epsilon(x - \lambda), \\ \epsilon' &= 0, \\ \lambda' &= 0. \end{aligned} \quad (27)$$

Now, for the remainder of the section, we apply the method of ? to the Van der Pol System. The canonical form for 24 is,

$$\begin{aligned} x' &= -yh_1(x, y, \epsilon, \lambda) + x^2h_2(x, y, \epsilon, \lambda) + \epsilon h_3(x, y, \lambda, \epsilon) \\ &= -y + x^2 \left(1 - \frac{x}{3}\right), \\ y' &= \epsilon(xh_4(x, y, \epsilon, \lambda) - \lambda h_5(x, y, \epsilon, \lambda) + yh_6(x, y, \lambda, \epsilon)) \\ &= \epsilon(x - \lambda). \end{aligned} \quad (28)$$

It follows that $h_1 = 1$, $h_2 = 1 - \frac{x}{3}$, $h_3 = 0$, $h_4 = 1$, $h_5 = 1$ and $h_6 = 0$. To simplify the following computations, we define

$$\begin{aligned} a_1 &= \frac{\partial}{\partial x} h_3(0, 0, 0, 0) = 0, \quad a_2 = \frac{\partial}{\partial x} h_1(0, 0, 0, 0) = 0, \quad a_3 = \frac{\partial}{\partial x} h_2(0, 0, 0, 0) = -\frac{1}{3}, \\ a_4 &= \frac{\partial}{\partial x} h_4(0, 0, 0, 0) = 0, \quad a_5 = h_6(0, 0, 0, 0) = 0. \end{aligned}$$

Furthermore, we can define the quantity,

$$A = -a_2 + 3a_3 - (2a_4 + 2a_5) = -1,$$

which is important in the following analysis, in particular for $A \neq 0$ (?). Similar to the procedure in Section 3, sections of the dynamical system can be defined, in order to monitor the in- and outgoing trajectories. In this case we are interested in two sections of the neighbourhood U , defined as in Section 3, that monitor S^a and S^r close to the fold point. Let $\Delta_a = \{(x, \rho^2), x \in I_a\}$ and $\Delta_r = \{(x, \rho^2), x \in I_r\}$, where I_a, I_r are intervals on the real line and ρ is sufficiently small. Furthermore, define q_a to be the point on Δ_a that belongs to the attracting branch S^a , while q_r is equivalently defined as the point on Δ_r that corresponds to S^r . Finally, we are in the position to define the transition map $\pi : \Delta^a \rightarrow \Delta^r$, compare to Section 3. Following this, ? discuss the existence of a critical value for λ (denoted λ_c), where the two branches S_r and S_a must connect in a smooth fashion. The transition map π has to map the point p_a to p_r , if the branches are connected, and the trajectory passing through the fold point is called the maximal canard, see Definition 4.2. The theorem below describes the technical details involved, and some of the results are derived by the following analysis.

Theorem 4.4 (?)

Assume that system (3.1) satisfies the defining non-degeneracy conditions (Equations 25 and 26) of a canard point. Assume that the maximal solution of the reduced problem connects S_a to S_r . Then there exists $\epsilon_0 > 0$ and a smooth function $\lambda_c(\sqrt{\epsilon})$ defined on $[0, \epsilon_0]$ such that for $\epsilon \in (0, \epsilon_0)$ the following assertions hold:

- $\pi(q_{a,\epsilon}) = q_{r,\epsilon}$ iff $\lambda = \lambda_c(\sqrt{\epsilon})$.
- The function λ_c has the expansion

$$\lambda_c(\sqrt{\epsilon}) = -\epsilon \left(\frac{a_1 + a_5}{2} + \frac{A}{8} \right) + O\left(\epsilon^{\frac{3}{2}}\right).$$

- The transition map π is defined only for λ in an interval around $\lambda_c(\sqrt{\epsilon})$ of width $O(\exp(-\frac{c}{\epsilon}))$ for some $c > 0$.

$$\left. \frac{\partial}{\partial \lambda} (\pi(q_{a,\epsilon}) - q_{r,\epsilon}) \right|_{\lambda=\lambda_c(\sqrt{\epsilon})} > 0$$

4.1 The Blow-Up Method on the Canard Point

Now similarly to Section 3, we consider a transformations of the coordinate system in order to analyse the dynamics in the neighbourhood of the non-hyperbolic equilibrium induced by the canard point. The transformations are taken from (?) and are,

$$x = \bar{r}\bar{x}, \quad y = \bar{r}^2y, \quad \epsilon = \bar{r}^2\bar{\epsilon}, \quad \lambda = \bar{r}\bar{\lambda}. \quad (29)$$

Now that we have established these transformation, the charts K_1 and K_2 can be introduced, but it is not necessary to consider the third chart, K_3 . Since the attracting slow manifold connects to the repelling slow manifold, the flow will ‘bend back’ from K_2 into K_1 instead of leaving the neighbourhood U in the direction of the fast flow, which was described by K_3 in Section 3. The trajectory stays close to S^r after passing the fold point. This is very counter-intuitive as the trajectory stays close to a repelling branch.

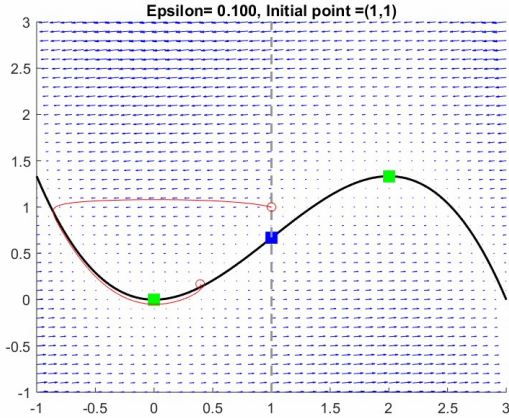


Figure 11: The Van der Pol system for the canard case.

Again, equivalently to the procedure in Section 3, we can define the coordinate transformation for the charts. Note, that in contrast to the generic Blow-Up in Section 3, the coordinate system is now in \mathbf{R}^4 , and not in \mathbf{R}^3 . In chart K_1 , $y_1 = 1$, while in K_2 , $\epsilon_1 = 1$ and then:

$$x = r_1 x_1, \quad y = r_1^2, \quad \epsilon = r_1^2 \epsilon_1, \quad \lambda = r_1 \lambda_1 \quad (30a)$$

$$x = r_2 x_2, \quad y = r_2^2 y_2, \quad \epsilon = r_2^2, \quad \lambda = r_2 \lambda_2. \quad (30b)$$

Furthermore, we can define the coordinate change between the two charts as follows:

Lemma 4.5

Let κ_{12} denote the change of coordinates from K_1 to K_2 . Then κ_{12} is given by

$$x_2 = x_1 \epsilon_1^{-1/2}, \quad y_2 = \epsilon_1^{-1}, \quad r_2 = r_1 \epsilon_1^{1/2}, \quad \lambda_2 = \epsilon_1^{-1/2} \lambda_1,$$

for $\epsilon_1 > 0$. Similarly $\kappa_{21} = \kappa_{12}^{-1}$ is given by

$$x_1 = x_2 y_2^{-1/2}, \quad r_1 = r_2 y_2^{1/2}, \quad \epsilon_1 = y_2^{-1}, \quad \lambda_1 = \lambda_2 y_2^{-1/2},$$

for $y_2 > 0$.

We are now in the position to begin with the analysis in the charts, and will first consider chart K_2 , since, as in Section 3, K_2 holds the most information.

4.1.1 Dynamics in K_2

Equivalently to Section 3, we rescale time such that, $\frac{dr}{dt_2} = \frac{dt}{dt_2} \frac{dr}{dt} = \frac{1}{r_2} \frac{dr_2}{dt}$. Then if we substitute the time transformation and Equation 30b into system 24 we find,

$$x'_2 = -y_2 + x_2^2 - r_2 G_1(x_2, y_2) = -y_2 + x_2^2 - r_2 \left(-\frac{x_2^3}{3} \right), \quad (31a)$$

$$y'_2 = x_2 - \lambda_2 + r_2 G_2(x_2, y_2) = x_2 - \lambda_2, \quad (31b)$$

where $G(x_2, y_2) = (G_1(x_2, y_2), G_2(x_2, y_2))^T = \left(-\frac{x_2^3}{3}, 0 \right)^T$. Moreover, ? discusses that for this chart we have an interesting result. They note that at $r_2 = \lambda_2 = 0$ the system is integrable which allows us to define a constant of motion $H(x_2, y_2) = \frac{1}{2} \exp(-2y_2) (y_2 - x_2^2 + \frac{1}{2})$. For clarity we will first proceed with deriving this equation of motion. Firstly, multiply each equations by, $e^{2y_2} e^{-2y_2} = 1$, and define sections of each equation as partial derivatives of H such that,

$$x'_2 = e^{2y_2} e^{-2y_2} (-y_2 + x_2^2) = e^{2y_2} \frac{\partial H}{\partial y_2}(x_2, y_2) \quad (32)$$

$$y'_2 = -e^{2y_2} e^{-2y_2} (-x_2) = -e^{2y_2} \frac{\partial H}{\partial x_2}(x_2, y_2). \quad (33)$$

Then we integrate $\frac{\partial H}{\partial x_2}(x_2, y_2) = -e^{-2y_2} x_2$ to give,

$$H(x_2, y_2) = -\frac{1}{2} x_2^2 e^{-2y_2} + C(y),$$

where $C(y)$ is the constant of integration, which depends on y . Then, by taking the derivative with respect to y and setting it equal to the expression $\frac{\partial H}{\partial y_2}(x_2, y_2) = e^{-2y_2}(-y_2 + x_2^2)$, we can find the value for $C(y)$ as follows:

$$\begin{aligned}\frac{\partial H}{\partial y_2}(x_2, y_2) &= x_2^2 e^{-2y_2} + C'(y) \\ \Rightarrow C'(y) &= -y_2 e^{-2y_2}\end{aligned}$$

Finally we integrate $C'(y)$ in order to find an explicit expression for H ,

$$C(y) = \int -y_2 e^{-2y_2} dy = \frac{1}{2} y_2 e^{-2y_2} + \frac{1}{2} e^{-2y_2} + \text{const},$$

using integration by parts. Then, the final expression is:

$$H(x_2, y_2) = -\frac{1}{2} x_2^2 e^{-2y_2} + \frac{1}{2} y_2 e^{-2y_2} + \frac{1}{2} e^{-2y_2} + c \quad (34)$$

$$= \frac{1}{2} e^{-2y_2} \left(y_2 - x_2^2 + \frac{1}{2} \right) + c. \quad (35)$$

Note that without loss of generality we can choose $c = 0$ because we are interested in the level curves of $H(x_2, y_2) = h$. The reduced system has an equilibrium of center type at the origin. Around this point, the level curves of $H = h$ for $h \in (0, \frac{1}{4})$ define periodic trajectories orbiting the equilibrium. When $h \leq 0$, the solutions are unbounded. When $h = 0$, we have that $y_2 - x_2^2 + \frac{1}{2} = 0$ and therefore,

$$x'_2 = \frac{1}{2} \implies x_2 = \frac{t_2}{2} + B, \quad (36a)$$

$$y'_2 = \frac{t_2}{2} \implies y_2 = \frac{t_2^2}{4} - \frac{1}{2}, \quad (36b)$$

where we have directly integrated Equation(36a) with respect to the rescaled time t_2 . However, we note that we are able to choose $B = 0$, as we are considering an autonomous (time-invariant) system. Using Equations (36a) and (36b) we are then able to define $\gamma_{c,2}$ as,

$$\gamma_{c,2}(t_2) = (x_{c,2}(t_2), y_{c,2}(t_2)) = \left(\frac{t_2}{2}, \frac{t_2^2}{4} - \frac{1}{2} \right). \quad (37)$$

This is the candidate trajectory in K_2 that perturbs to a maximal canard trajectory. Now that we have established that we must have a flow on the second chart, there must also exist transition maps. Therefore this now enables us to consider the first chart in the following section.

4.1.2 Dynamics in K_1

For K_1 we follow a similar approach to the above. We will use the transformations,

$$x = r_1 x_1, \quad y = r_1^2, \quad \epsilon = r_1^2 \epsilon_1, \quad \lambda = r_1 \lambda_1, \quad (30a)$$

to find the relevant trajectory γ_1 corresponding to γ_2 in K_2 . Now if we first consider the r_1 component,

$$\begin{aligned} 2r_1^2 r'_1 &= r_1^2 \epsilon_1 (r_1 x_1 - r_1 \lambda_1), \\ \Rightarrow r'_1 &= \frac{1}{2} \epsilon_1 r_1 (x_1 - \lambda_1) = \frac{1}{2} \epsilon_1 r_1 F, \end{aligned} \quad (38)$$

where $F = F(x_1, y_1, \epsilon_1, \lambda_1) = x_1 - \lambda_1$. Next we consider $x = r_1 x_1$,

$$\begin{aligned} r_1 r'_1 x_1 + r_1^2 x'_1 &= -r_1^2 + r_1^2 x_1^2, \\ \Rightarrow x'_1 &= -1 + x_1^2 - \frac{x_1 r'_1}{r_1}, \end{aligned}$$

and substituting in the expression for r'_1 results in,

$$x'_1 = -1 + x_1^2 - \frac{x_1}{r_1} \left(\frac{r_1 \epsilon_1 F}{2} \right). \quad (39)$$

We now consider $\epsilon = \epsilon_1 r_1^2$ and noting $\epsilon' = 0$. Then we have, $r_1^3 \epsilon' = -2r_1^2 \epsilon_1 r'_1$, where we can use Equation (38) to simplify to,

$$\epsilon' = -\epsilon_1^2 F. \quad (40)$$

The last transformation is for the new coordinate $\lambda = r_1 \lambda$, noting that $\lambda' = 0$. Similarly to the above we find $r_1^2 \lambda'_1 + r_1 \lambda_1 r'_1 = 0$ then,

$$\lambda'_1 = -\frac{\lambda_1 \epsilon_1 F}{2}, \quad (41)$$

which is a trivial rearrangement as seen in Equation 40. Now if we combine the above we find that the transformed system is of the following form,

$$r'_1 = \frac{\epsilon}{2} r_1 F, \quad (42a)$$

$$x'_1 = -1 + x_1^2 - \frac{x_1 \epsilon_1 F}{2},$$

$$\epsilon' = -\epsilon_1^2 F, \quad (42b)$$

$$\lambda'_1 = -\frac{\lambda_1 \epsilon_1 F}{2}.$$

From this system we are now able to make some deductions. We first can observe that the hyperplanes are along the $r_1 = \epsilon_1 = \lambda_1 = 0$ which intersect in the invariant line at $l_1 = \{(x_1, 0, 0, 0) : x_1 \in \mathbb{R}\}$ (?). As ? discusses, the equilibria are located at the end of both branches - Figure 9 - which are found at $p_a = (-1, 0, 0, 0)$ and $p_r = (1, 0, 0, 0)$. We can find the eigenvalues of equation (42) for the invariant planes. We find that,

$$J - \sigma I = \begin{bmatrix} 2x - \sigma & 0 & 0 & 0 \\ 0 & -\sigma & 0 & 0 \\ 0 & 0 & -\sigma & 0 \\ 0 & 0 & 0 & -\sigma \end{bmatrix}, \quad (43)$$

which has three zero eigenvalues and one non-zero eigenvalue $\sigma = \pm 2$. This further emphasises that the equilibrium point is non-hyperbolic. The dynamics of K_1 is very similar to the analysis of K_1 in the generic fold case. The center manifold can be applied in order to conclude the persistence of the dynamics for $\epsilon > 0$.

4.2 Full Solution

The analysis of the charts K_1 and K_2 provided enough hyperbolicity in order to conclude persistence of the special orbit γ for $\epsilon > 0$. The orbit γ connects the attracting and repelling branch of S at p_a and p_r . This can be observed in Figure 12, which shows the full local dynamics at the fold point. We

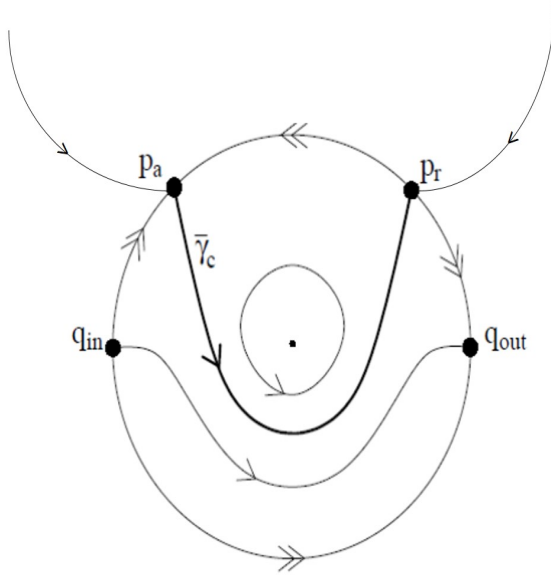


Figure 12: Full dynamics at the fold point in the canard case (?).

now would like to understand the effect this connection of manifolds at the fold point has on the global dynamics of the system.

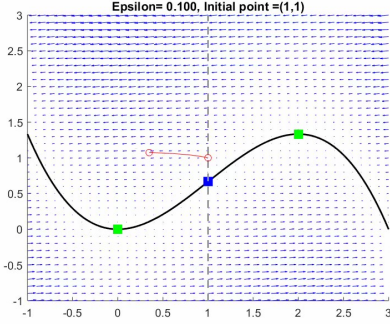
4.3 Effect of the Canard Point

Now that we have shown that there must exist a flow around the fold point we should now consider the global effect of the canard trajectory. We can see by considering the system of equations (27) that the equilibrium of the system is at $(x, y) = (\lambda, \lambda^2[\frac{1-\lambda}{3}])$ and depends on λ , as expected. We can find the eigenvalues from the matrix,

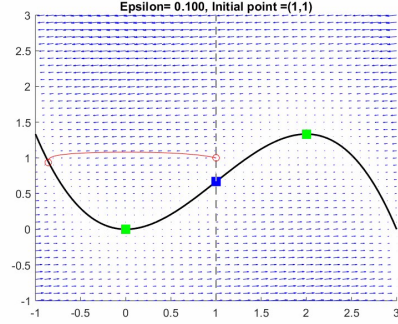
$$A - \sigma I = \begin{bmatrix} 2x - x^2 - \sigma & -1 & 0 & 0 \\ \epsilon & -\sigma & x - \lambda & -\epsilon \\ 0 & 0 & -\sigma & 0 \\ 0 & 0 & 0 & -\sigma \end{bmatrix} = \sigma^2(\sigma^2 + \sigma(x^2 - 2x) + \epsilon). \quad (44)$$

The eigenvalues of the system are $\sigma = 0$ and $\sigma = \frac{2x-x^2 \pm \sqrt{(x^2-2x)^2-4\epsilon}}{2}$. Then we consider the values at the equilibrium, $x = \lambda$, to find that we have a Hopf Bifurcation when $4\epsilon > (x^2 - 2x)^2$ or when $\lambda = 2$ or 0 . The Hopf bifurcation is not a surprising occurrence since it represents a change in stability of an equilibrium. Since the equilibrium of the reduced system changes from stable to relaxation oscillations at the fold points, some bifurcation can be expected at those point. This then leads to the following trajectories within the flow - Figure 13.

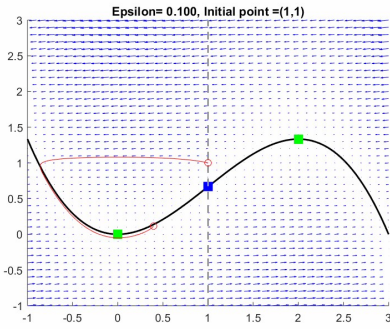
4. CANARDS IN TWO DIMENSIONS



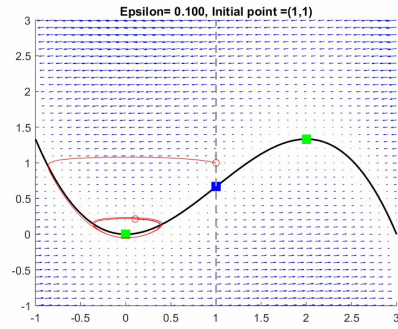
(a) The initial flow within the system.



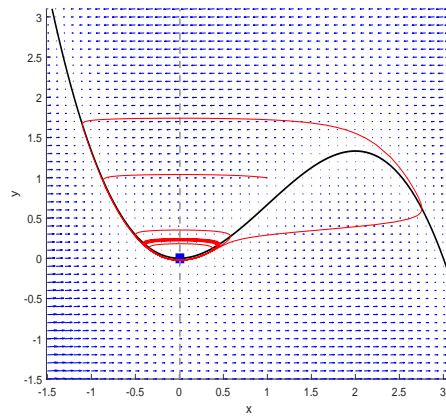
(b) The flow as it hits the slow manifold.



(c) The flow as it intersects with the fold point.



(d) The Hopf bifurcation due to the canard point.



(e) Growth of the Hopf bifurcation leading to the formation of a Canard explosion.

Figure 13: The trajectories associated with the canards case of the Van der Pol system.

From Figure 13 we can see the progression of the flow over the system. From Figure 13a we see that the flow starts at an initial condition of $(x, y) = (1, 1)$ and travels along the fast flow towards the

attracting branch. Then in Figure 13b the flow has hit the attracting branch, where it then follows along the slow flow towards the fold point at $(x, y) = (0, 0)$, which is described by Figure 13c. Then from Figures 13c and 13d we can observe the Hopf bifurcation. These small amplitude oscillations are the perturbation of the closed orbits due to the constant of motion found in the singular limit in chart 2. It can be seen that the trajectories follow the repelling branch (see Figure 9) until the flow is sufficiently far from the fold point where it will then repel towards the attracting branch - Figure 13d. For increasing values of λ , the canard cycles get larger and trajectories that follow the repelling branch are either repelled towards the left or the right - Figure 13e. The canards jumping off the repelling branch to the right are called canards with head because of the shape they trace out. The question whether trajectories jump off to the left or to the right is answered by investigating the separation of the manifolds.

4.3.1 Separation of the Manifolds

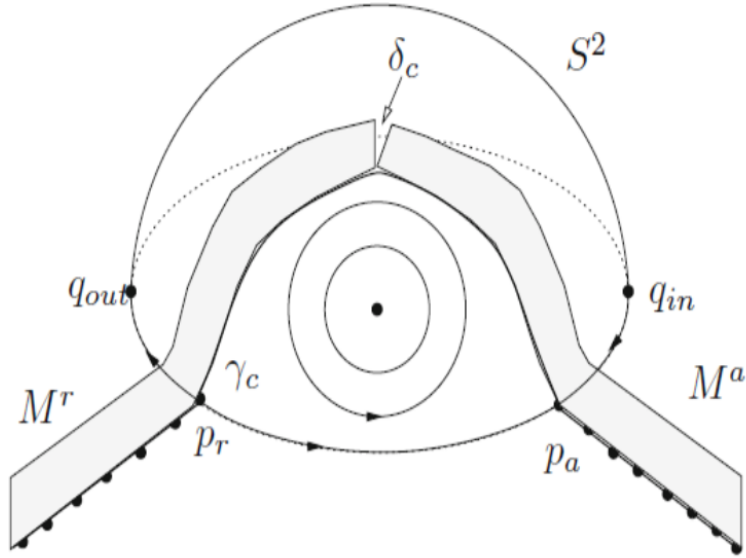


Figure 14: Separation of M_a and M_r (?).

The maximal canard connects the attracting and repelling branches of the slow manifold as shown in Figure 14, where the trajectory is denoted by γ_c . However, for other values of λ than the critical value, the attracting and repelling branches are no longer connected, as shown in Figure 14. To measure the distance between the manifolds we will apply a Melnikov Computation - see ? for direct use. To discover whether we have a splitting between the attracting and repelling branches we need to consider the y coordinates in the second chart such that $y_{a,2}(0) - y_{r,2}(0)$ is a distance function, which can be written as $D_c(r_2, \lambda_2) = H(0, y_{a,2}(0)) - H(0, y_{r,2}(0))$. Note that $\frac{\partial}{\partial y_2} H(0, y_2) \neq 0$ (?). From here we can use the following proposition,

Proposition 4.6 (?)

For a small enough ρ and μ the distance function has the expansion

$$D_c(r_2, \lambda_2) = d_{r_2} r_2 + d_{\lambda_2} \lambda_2 + O(2),$$

with

$$d_{r_2} = \int_{-\infty}^{\infty} (\nabla H(\gamma_{c,2}(t)))^T \cdot G(\gamma_{c,2}(t)) dt, \quad (45a)$$

$$d_{\lambda_2} = \int_{-\infty}^{\infty} (\nabla H(\gamma_{c,2}(t)))^T \cdot (0, -1)^T, \quad (45b)$$

where the matrix $G(\gamma_{c,2}(t))$ is as defined in Section 4.1.2 and $\gamma_{c,2}$ is the trajectory associated with the singular canard.

Then, following the proof provided by ?, we find that we will have a split occurring between our branches if the canard falls outside of the domain of order $O(e^{-\frac{c}{\epsilon}})$ such that $D_c(r_2, \lambda_2) \neq 0$. We can calculate these explicitly for the Van der Pol system by using Equations 35, 37 and $G(x_2, y_2) = (-\frac{x_2^3}{3}, 0)^T$. Consequently we have,

$$\begin{aligned} d_{r_2} &= \int_{-\infty}^{\infty} \nabla \left(\frac{1}{2} e^{-2y_2} \left(y_2 - x_2^2 + \frac{1}{2} \right) \right)^T \cdot \left(\left(-\frac{x_2^3}{3}, 0 \right)^T \right) \Big|_{\gamma_{c,2}} dt, \\ &= -\frac{e}{16} \int_{-\infty}^{\infty} t^4 e^{-\frac{T^2}{2}} dt, \end{aligned}$$

noting $\nabla(H(\gamma_{c,2}(t))) = \exp(1 - \frac{t^2}{2}) [-1, \frac{1}{2}]$. Now the task is to show that d_{r_2} is finite, we do this by using integration by parts to find,

$$d_{r_2} = \frac{e}{16} \int_{-\infty}^{\infty} e^{-\frac{T^2}{2}} dt = \frac{e\sqrt{2\pi}}{16} < \infty, \quad (46)$$

where we note that we have made use of the Gaussian Integral (?) and d_{r_2} is finite. We then apply an analogous approach to d_{λ_2} such that ,

$$\begin{aligned} d_{\lambda_2} &= \int_{-\infty}^{\infty} \nabla \left(\frac{1}{2} e^{-2y_2} \left(y_2 - x_2^2 + \frac{1}{2} \right) \right)^T \cdot ((0, -1)^T) \Big|_{\gamma_{c,2}} dt, \\ &= -\frac{e}{2} \int_{-\infty}^{\infty} e^{-t^2} dt = -\frac{e\sqrt{2\pi}}{2} < 0, \end{aligned} \quad (47)$$

where we have used the same techniques as above and we can conclude that d_{λ_2} is also finite. Combining the above yields that the distance function is,

$$D_c(r_2, \lambda_2) = \frac{e\sqrt{2\pi}}{16} r_2 - \frac{e\sqrt{2\pi}}{2} \lambda_2 + O(2), \quad (48)$$

whereby we have that the manifolds in the Van der Pol system split for $\lambda_2 \neq \frac{r_2}{8}$. Otherwise the attracting and repelling branches are connected and the maximal canard exists. If the manifold splits

then we would find that the manifold is similar to Figure 14 whereby the flow will either jump off to the right - see Figure 13e - or the flow will be trapped in the canard region and then be repelled back to the attracting manifold, as we see with our connected system - Figure 13. The presence of either of these cases depends on how the manifold breaks. This describes the global dynamics for the region close to $\lambda = 0, \lambda = 2$. Therefore, we are now in the position to have a description of the full dynamics of the two dimensional Van der Pol System for all parameter regimes of λ . Since the canard solutions are restricted to an exponentially small region around the fold points, we now move on to three dimensional fast-slow systems, in which canards are more common occurrences.

5 Canards in Three Dimensions

Canards in two dimensional fast-slow systems are degenerate phenomena, while they generically occur in higher dimensional systems. This means that while in two dimensional systems canards only occur within an exponentially small region in parameter space. They occur in an $O(1)$ region for three dimensional systems and are therefore more robust. In the following two sections we consider three dimensional fast slow systems with one fast and two slow variables,

$$\begin{cases} \epsilon \dot{x} = f(x, y, z, y, \epsilon), \\ \dot{y} = g_1(x, y, z, y, \epsilon), \\ \dot{z} = g_2(x, y, z, y, \epsilon), \end{cases} \quad (49)$$

which is the original form of the fast-slow system (2), with $n = 1, m = 2$ (?). The analysis is of a similar structure as for the two dimensional case.

We can identify the points that will cause complication for the analysis of the system by considering the nondegeneracy conditions, as in the two dimensional case. Here, the extended version is

$$\begin{aligned} f(p_*, \lambda, 0) &= 0, \\ \frac{\partial}{\partial x} f(p_*, \lambda, 0) &= 0, \\ \frac{\partial^2}{\partial x^2} f(p_*, \lambda, 0) &\neq 0, \\ D_{(y,z)} f(p_*, \lambda, 0) \text{ has full rank one,} \end{aligned} \quad (50)$$

where $p_* = (x_*, y_*, z_*) \in F$ denotes the fold points and $D_{(y,z)} = \left(\frac{\partial f}{\partial y}, \frac{\partial f}{\partial z} \right)$ (?). This gives rise to a fold line, on which all of the fold points, p_* , lie. This consequence is immediately obvious by considering Figure 15, and projecting in to the $x - y$ plane we recover the 2-dimensional Van der Pol system. Then the two fold points in the two dimensional case extends to two fold lines in the three dimensional case. Further analysis need to be carried in order to find the points that are classified as folded singularities, denoted by * in Figure 15, giving rise to canard solutions. The criterion we need is the fact that a folded singularity coincides with an equilibrium of the desingularised reduced problem. Therefore, we

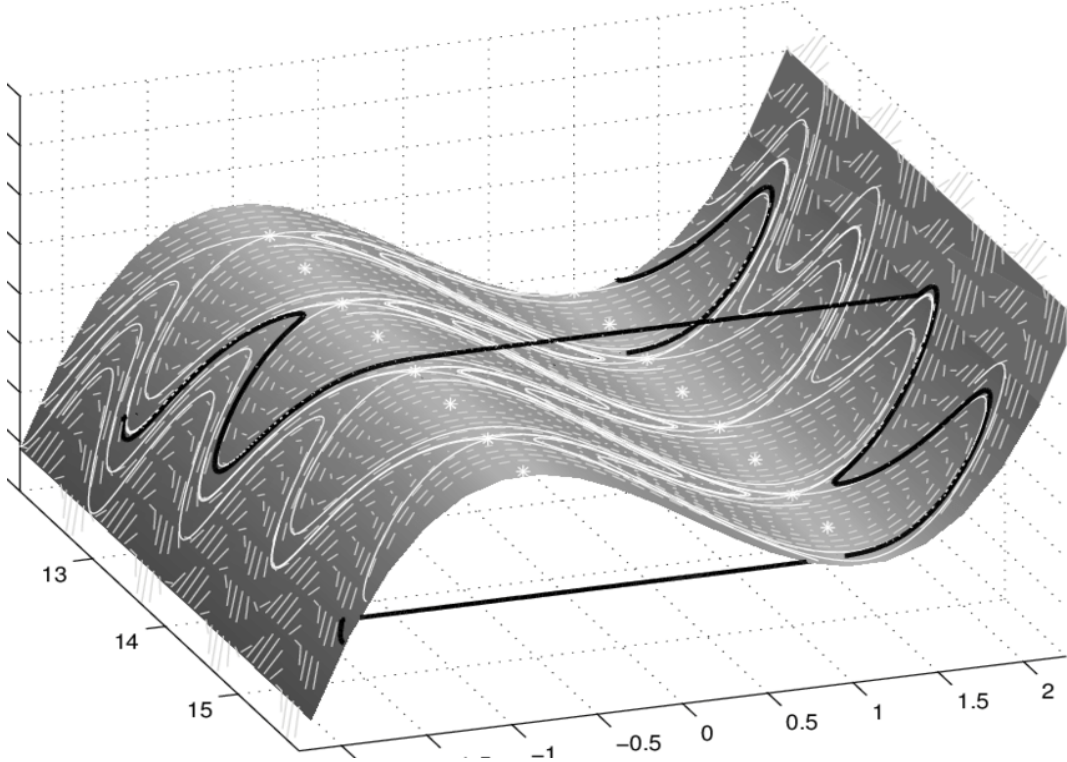


Figure 15: Three dimensional Van der Pol (?).

focus on the reduced system, as in the two dimensional case. The slow system (49) in the singular limit $\epsilon \rightarrow 0$ becomes,

$$\begin{cases} 0 &= f(x, y, z, y, \epsilon), \\ \dot{y} &= g_1(x, y, z, y, \epsilon), \\ \dot{z} &= g_2(x, y, z, y, \epsilon). \end{cases} \quad (51)$$

Now, taking the total derivative of f results in,

$$0 = \frac{df}{dt} = \dot{y} \frac{\partial f}{\partial y} + \dot{z} \frac{\partial f}{\partial z} + \dot{x} \frac{\partial f}{\partial x}.$$

Then, rearranging for the term including \dot{x} and noting that $y' = g_1$ and $z' = g_2$ results in

$$-\dot{x} \frac{\partial f}{\partial x} = g_1 \frac{\partial f}{\partial y} + g_2 \frac{\partial f}{\partial z}.$$

This is almost of the desired form, however, we cannot divide by $-\frac{\partial f}{\partial x}$ to get an expression for \dot{x} , since $\frac{\partial f}{\partial x}(p_*) = 0$, from the nondegeneracy condition. Therefore, as in the two dimensional case, we apply a rescaling of time in terms of $-\frac{\partial f}{\partial x}$, such that

$$\begin{cases} \dot{x} &= g_1 \frac{\partial f}{\partial y} + g_2 \frac{\partial f}{\partial z}, \\ \dot{y} &= -g_1 \frac{\partial f}{\partial x}, \\ \dot{z} &= -g_2 \frac{\partial f}{\partial x}. \end{cases} \quad (52)$$

This is the desingularised reduced system, and its equilibrium satisfies

$$l(p^*) = g_1(p_*, \lambda, 0) \frac{\partial}{\partial y} f(p_*, \lambda, 0) + g_2(p_*, \lambda, 0) \frac{\partial}{\partial z} f(p_*, \lambda, 0) = 0.$$

This is where the so called transversality condition $l(p_*) \neq 0$ fails (?). This condition means that the desingularised flow is not tangent to the fold curve at p_* . The next step is to consider the nature of the folded singularity. This was not as relevant in the two dimensional system, however, in the three dimensional case, the type of equilibrium the reduced system possesses determines the type and number of canards that can be observed in the full system. Therefore, we consider the three dimensional Jacobian,

$$J = \begin{bmatrix} \frac{\partial \dot{x}}{\partial x} & \frac{\partial \dot{x}}{\partial y} & \frac{\partial \dot{x}}{\partial z} \\ \frac{\partial \dot{y}}{\partial x} & \frac{\partial \dot{y}}{\partial y} & \frac{\partial \dot{y}}{\partial z} \\ \frac{\partial \dot{z}}{\partial x} & \frac{\partial \dot{z}}{\partial y} & \frac{\partial \dot{z}}{\partial z} \end{bmatrix}. \quad (53)$$

The resulting three eigenvalues, σ_i for $i = 1, 2, 3$ determine the stability of the folded singularity (?). Without loss of generality we can choose $\sigma_3 = 0$, because at least one of the eigenvalues must be zero to account for the folded singularity. The other two eigenvalues can be defined as the weak and strong eigenvalues, corresponding to the weak and strong canards, introduced below. This classification of the eigenvalues is done as follows: $|\sigma_1| > |\sigma_2| \iff |\sigma_s| > |\sigma_w|$, meaning that the eigenvalue with the largest modulus is called the strong eigenvalue and vice versa. We define the eigenvalue ratio $\mu := \frac{\sigma_w}{\sigma_s}$. We can infer from standard stability theory that the folded singularity can have three types of stability, classified as follows (?),

$$\begin{cases} \text{Saddle } \sigma_1 \sigma_2 < 0 : \sigma_i \in \mathbf{R}, \\ \text{Node } \sigma_1 \sigma_2 > 0 : \sigma_i \in \mathbf{R}, \\ \text{Focus } \sigma_1 \sigma_2 > 0 : \text{Im}(\sigma_i) \neq 0. \end{cases} \quad (54)$$

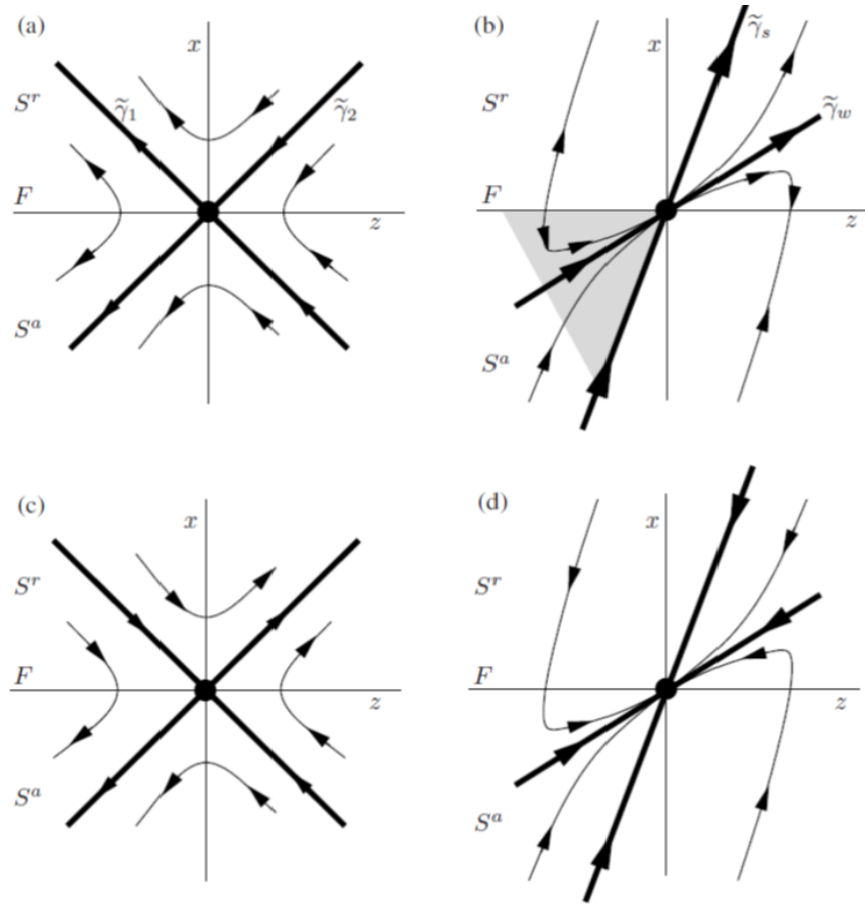


Figure 16: Phase portraits around the singularities of our three dimensional system where they are a) a folded saddle and b) folded node. Corresponding desingularised flows are shown in c) and d) (?).

Two of the three types of equilibria are illustrated in Figure 16, where the effect of the desingularisation is displayed as well. The scaling by $-\frac{\partial f}{\partial x}$ causes a reversal of the arrows in the repelling sheet S^r , which allows the two trajectories passing through the folded singularity to connect the attracting and repelling sheet which is not possible before desingularisation. These connecting trajectories are called singular canards.



Figure 17: The branches of a spiral (?).

It should be noted that a singular canard is only present if the node or saddle connects the attracting and repelling sheets S^r and S^a . However, for the focus equilibrium we are unable to construct branches which connect, since the trajectories are strictly spiralling towards or away from the equilibrium, consider Figure 17. Then, desingularising the flow, which causes the reversal of the flow on the repelling sheet will only have the effect that the spiralling trajectories cannot cross the fold. Therefore, there are no singular canards present in the case of a folded focus.

The following theorem summarises the findings for the different types of equilibria and the presence of canards in three dimensions.

Theorem 5.1 (Canards in \mathbf{R}^3 (?)

For fast-slow systems (Equation 49) with $\epsilon > 0$ sufficiently small the following holds:

1. There are no maximal canards generated by a folded focus. For a folded saddle the two singular canards $\bar{\gamma}_{1,2}$ perturb to maximal canards $\gamma_{1,2}$.
2. For a folded node let $\mu = \frac{\sigma_w}{\sigma_s} < 1$. the singular canard $\bar{\gamma}_s$ (“the strong canard”) always perturbs to a maximal canard γ_s . If $\mu^{-1} \notin \mathbb{N}$, then the singular canard $\bar{\gamma}_w$ (“weak canard”) also perturbs to a maximal canard. We call γ_s and γ_w primary canards.
3. For a folded node suppose $k > 0$ is an integer such that $2k+1 < \mu^{-1} < 2k+3$ and $\mu^{-1} \neq 2(k+1)$. Then, in addition to $\gamma_{s,w}$ there are k other maximal canards, which we call secondary canards.
4. The primary weak canard of a node undergoes a transcritical bifurcation for odd $\mu^{-1} \in \mathbb{N}$ and a pitchfork bifurcation for even $\mu^{-1} \in \mathbb{N}$

This theorem summarises the findings for different types of folded singularities. It establishes the persistence of the singular canards as maximal canards of the full system $\epsilon > 0$ for the different types of singularities. Furthermore, it provides a tool for calculating the number of secondary canards present in the full system, additional to the primary canards γ_s and γ_w . For $\mu^{-1} \in \mathbb{N}$ bifurcations occur and the number of secondary canards present varies according to the type of bifurcation. These mechanisms are best understood in the case of a folded node, which is studied in the following section.

5.1 The Folded Node

In this section the occurrence of canards and small amplitude oscillations (SAOs) due to a folded node of the reduced system is discussed. For a full presentation of canards in three dimensions for a folded node, see *Canards in \mathbf{R}^3* by ?. The folded node singularity is an equilibrium of the reduced system. Note that it is only defined on S , the critical manifold and not the full system. There is no global equilibrium for the normal form introduced below. The normal form considered for analysis of the

folded node singularity is,

$$\begin{aligned}\epsilon \dot{x} &= y - x^2, \\ \dot{y} &= -z - (\mu + 1)x, \\ \dot{z} &= \frac{1}{2}\mu,\end{aligned}\tag{55}$$

where μ is the eigenvalue ratio. Note here that the reason that no global equilibrium exists is because System (55) can only have an equilibrium if $\dot{z} = 0$. This would imply that $\mu = 0$. However, as the classification of folded singularities has shown, since $\sigma_1\sigma_2 > 0$, $\mu \neq 0$ for the folded node. It is now of interest to verify the location of the folded singularity at the origin, and therefore derive the reduced system as well as the eigenvalues for the reduced problem. This is a simple application of the theory introduced earlier in this section. Consider equation (55) and define $\dot{x} := f$ as before. When $\epsilon \rightarrow 0$ in system (55), it follows that $f = y - x^2 = 0$, and therefore the critical manifold is defined as $S := \{(x, y, z) : y = x^2\}$, which is a folded two dimensional plane. Now that f is defined explicitly, we can check the nondegeneracy conditions for a folded singularity, as presented in (50) and get the following results,

$$f(x, y, z, , \mu, \epsilon) = 0,$$

$$\implies y = x^2,$$

$$\frac{\partial f}{\partial x}(x, y, z, \mu, \epsilon) = 2x = 0,$$

$$\implies x = 0,$$

$$\implies y = 0,$$

$$\frac{\partial^2 f}{\partial x^2}(x, y, z, \mu, \epsilon) = 2 \neq 0,$$

$$D_{(y,z)}f = (1, 0) \text{ full rank one.}$$

This shows that there exists a fold line $L := (0, 0, z)$ on the slow manifold S . In order to determine at which value of z the folded node singularity is located, we have to consider the reduced system of (55). The aim is to find an equilibrium of the reduced problem, since we know from the theory discussed that the folded singularity is an equilibrium of the slow flow. The reduced problem is,

$$0 = y - x^2 := f, \tag{56}$$

$$\dot{y} = -z - (\mu + 1)x, \tag{57}$$

$$\dot{z} = \frac{1}{2}\mu. \tag{58}$$

We are interested in the global dynamics of the slow system and therefore want to derive an expression for \dot{x} . In order to do so, as described earlier in this section, we take the total derivative of f and rearrange to get the following expression,

$$\dot{y} = 2x\dot{x}. \quad (59)$$

This can be rearranged to give an expression for the dynamics in x on the slow manifold,

$$\dot{x} = \frac{\dot{y}}{2x},$$

which is singular for $x = 0$, coinciding with the fold line. This can be desingularised by rescaling time in the whole reduced system by a factor of $2x$. This results in,

$$\begin{aligned}\dot{x} &= -(\mu + 1)x - z, \\ \dot{y} &= -2x(\mu + 1) - 2xz, \\ \dot{z} &= x\mu.\end{aligned} \quad (60)$$

However it can be noted that the equation for y can be omitted, since the change in y is directly related to the change in x by a factor of $2x$ as stated in Equation 59. Therefore, the reduced dynamics can be sufficiently described by,

$$\begin{aligned}\dot{x} &= -(\mu + 1)x - z, \\ \dot{z} &= x\mu.\end{aligned} \quad (61)$$

Now, following the theory for folded singularities, the folded node has to satisfy the condition $l(0, 0, z) = 0$, such that

$$\begin{aligned}l(0, 0, z) &= -(\mu + 1)x - z = 0|_{(0, 0, z)}, \\ \Rightarrow z &= 0.\end{aligned}$$

This leads us to the conclusion that the folded singularity, defined on the slow manifold for $\epsilon \rightarrow 0$ and located on the fold line $L = (0, 0, z)$, is given by $(0, 0, 0)$, as expected. Note that in this case only one equilibrium of the reduced system exists, which is not necessarily the case. The next step of the analysis is to verify that the folded singularity at the origin is indeed a folded node. As discussed in the beginning of Section 5, the classification of the singularities is determined by the eigenvalues of the reduced system. Therefore, the next step is calculating these eigenvalues. The Jacobian of the reduced system (61) is

$$J = \begin{bmatrix} -(\mu + 1) & -1 \\ \mu & 0 \end{bmatrix}, \quad (62)$$

and therefore the characteristic equation yields

$$\begin{aligned}\sigma^2 + (\mu + 1)\sigma + \mu &= 0, \\ \implies \sigma_1 &= -1 \quad \text{and} \quad \sigma_2 = -\mu.\end{aligned}$$

Since μ is the eigenvalue ratio and satisfies $0 < \mu < 1$, we can conclude that $\sigma_1\sigma_2 = (-1)(-\mu) = \mu > 0$ and the folded singularity is in fact a folded node. Note that if we had tried to find the eigenvalues for the full three dimensional reduced system (60) instead, an additional eigenvalue $\sigma_3 = 0$ would have occurred. This is the eigenvalue that corresponds to the loss of hyperbolicity at the folded node, which is expected for singular points.

In order to analyse the folded node, the system (55) is transformed using the blow up transformation $u = \epsilon^{1/2}\bar{x}$, $v = \epsilon\bar{y}$, $w = \epsilon^{1/2}\bar{z}$ and $\tau_1 = \epsilon^{1/2}\bar{t}$. Then, in a neighbourhood U of the folded node, the system is represented by,

$$\begin{aligned}\dot{x} &= \bar{y} - \bar{x}^2, \\ \dot{y} &= \bar{z} - \bar{x}, \\ \dot{z} &= -\nu,\end{aligned}$$

where ν satisfies $\nu = \frac{\mu}{2(1+\mu)^2}$. In the following analysis the bars will be omitted for convenience. One important realisation is that the phase portraits for the rescaled system are topologically equivalent to the original normal form. Therefore, the mapping of solutions found in the blown up system to the original system is straightforward.

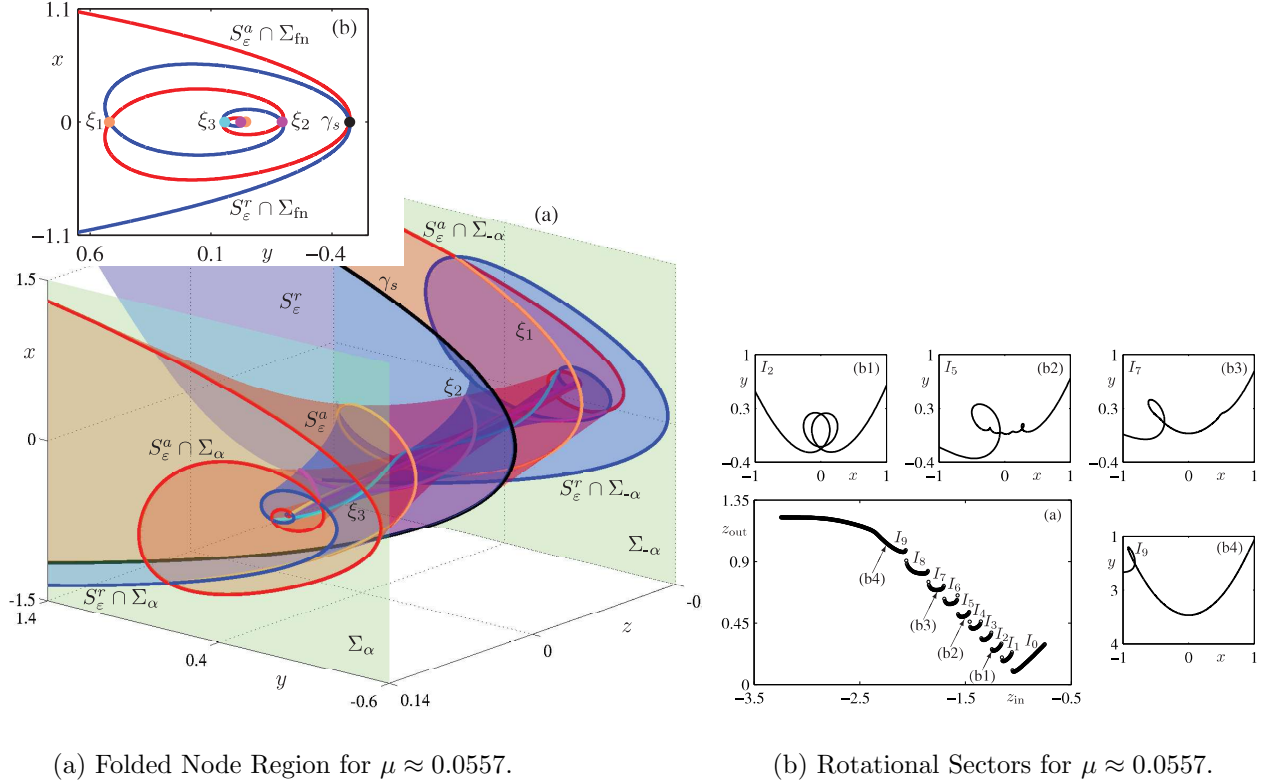
All the information needed to describe the dynamics near the fold point is now derived and therefore the next step in the analysis is the description of the small amplitude oscillations (SAOs). The SAOs in the folded node case are canard trajectories that follow a certain pattern. These patterns are, as discussed in Theorem 5.1, found by considering the eigenvalue ratio μ . In the case of the folded node, μ satisfies $2k+1 < \mu^{-1} < 2k+3$. Solving for $k \in \mathbf{N}$ gives that k is the number of secondary canards ξ_i , where $i \in 1, \dots, k$, in the system - stated in Theorem 5.1. Furthermore, k corresponds to the number of twists the primary canard γ_s is performing around γ_w . A twist corresponds to a 180° rotation, see ?. In order to derive the number of secondary canards, $\mu^{-1} \notin \mathbf{N}$ has to be satisfied. If $\mu^{-1} \in \mathbf{N}$, bifurcations occur and the number of secondary canards changes. For a full analysis of this phenomenon refer to ?.

These canards are trajectories that are entering the so called funnel region of the fold and contracted along the direction of S^a . This funnel region lies between the fold line L and the strong singular canard. It is represented by the grey shaded region in Figure 16. For decreasing values of ϵ , the funnel becomes narrower and for $\epsilon \rightarrow 0$, all other canards converge to the strong singular canard. The number of SAOs an incoming trajectory undergoes depends on where the trajectory enters the fold region in the z plane. Different intervals I_i , $i \in 1, \dots, k$, of z can be defined according to how many SAOs will be observed in the interval. The interval in which the primary strong canard lies is significantly larger than the other intervals, so the secondary canards close to it will have a higher amplitude while the number of SAOs is smaller. As the number of SAOs increases, the amplitude of oscillations get smaller and are not readily visible. The result about the width of the intervals is summed up in the following

theorem.

Theorem 5.2 (Width of Rotational Sectors (?))

Consider system (52) and assume it has a folded-node singularity. At an $O(1)$ distance from the fold curve, all secondary canards are in an $O(\epsilon^{(1-\mu)/2})$ neighbourhood of the primary strong canard. Hence, the width of the rotational sectors $I_i, 1 \leq i \leq k$, is $O(\epsilon^{(1-\mu)/2})$ and the width of sector I_{k+1} is $O(1)$.



(a) Folded Node Region for $\mu \approx 0.0557$.

(b) Rotational Sectors for $\mu \approx 0.0557$.

Figure 18: Local dynamics around the folded node for $\mu \approx 0.0557$ (?).

? provides an illustrative example, where $\mu \approx 0.0557$ and therefore $k = 8$. Then, besides the strong and weak primary canards γ_s and γ_w , there exist eight secondary canards ξ_i , where $i \in 1, \dots, 8$. Figure 18a shows a small region of the phase space, which captures the intersection of the repelling and attracting sheet of the slow manifold. This region is bounded by two cross-sections, Σ^a and Σ^{-a} . Another cross-section Σ^{fn} can be defined, which corresponds to a two dimensional cross-section of the flow at the fold. This is displayed in Figure 18a. In the figure, the primary strong canard is illustrated in black, and the three strongest secondary canards are displayed as ξ_1 in orange, ξ_2 in magenta and ξ_3 in cyan. It is apparent, that the primary strong canard makes twists around the center, where the weak canard is located. The secondary canards ξ_i , $i \in 4, \dots, 8$, as well as γ_w are also present. However, they are not visible since they are increasingly close to each other in the middle.

The number of SAOs a trajectory undergoes is dependent on where it enters the funnel region in terms of the space variable z . The intervals that can be defined are I_0 up to I_9 , where I_0 is bounded by γ_s and much larger than the other intervals. The interval I_i , $i \in 1, \dots, 8$ is bounded by the corresponding number of secondary canards ξ_i to the left and ξ_{i-1} to the right, and entering the fold region through the i th interval corresponds to i oscillations a trajectory undergoes. This is illustrated in Figure 18b. This is only a very local picture of the dynamics present in system (55). Aspects of the global analysis are presented in the following section.

6 Global Return Mechanisms and Mixed Mode Oscillations

Before returning to the case of the folded node, a few technical terms are introduced in order to describe the relevant phenomena discussed in this section. This section is based on work done in the review paper by ? unless indicated otherwise. The first concept that we need to introduce is mixed mode oscillations (MMOs).

Definition 6.1. *Mixed Mode Oscillations* (?)

A mixed mode oscillation is an orbit γ , which traces out small amplitude oscillations (SAOs) as well as large amplitude oscillations (LAOs). The SAOs and LAOs are clearly separated in the time series and their recurrence can be periodic. The signature of an MMO is expressed as $L_1^{s_1} L_2^{s_2} \dots$, indicating that L number of LAOs are followed by s SAOs.

MMOs can be due to different mechanisms in the fast-slow system. They can be present due to a folded node singularity or a singular Hopf bifurcation, amongst others. We can now return to the example of the folded node and state some important results which give rise to MMOs for systems with folded node singularities.

6.1 The Folded Node

We have analysed the local behaviour of system (55) around the region close to the folded node. However, this does not provide the full analysis of the system, since the global behaviour of the trajectories

that undergo the SAOs in the folded node region is not captured by the local analysis. Generally, there are no global return mechanisms present in system (55) and a trajectory that approaches the folded region from $x = -\infty$ undergoes a number of SAOs, according to where it enters the fold region in z space, before leaving towards infinity. Then there are no global return mechanisms present and the trajectory does not undergo a large amplitude oscillation. However, there are certain criteria that indicate the existence of a global return mechanism and therefore that MMOs can be observed. There are two theorems related to this issue, which are stated below.

Theorem 6.2 (Generic 1^{k+1} MMOs ?)

Consider system (52) with the following assumptions:

1. Assume that $0 < \epsilon \ll 1$ is sufficiently small, $\epsilon^{1/2} \ll \mu$, and $k \in \mathbf{N}$ is such that $2k + 1 < \mu^{-1} < 2k + 3$.
2. The critical manifold S is (locally) a folded surface.
3. The corresponding reduced problem possesses a folded-node singularity.
4. There exists a candidate periodic orbit, which consists of fast fibres of the layer problem, a global return segment, and a segment on S^a within the funnel that starts at distance δ from $\bar{\gamma}_s$ (as measured at a distance $O(1)$ away from the fold F).
5. An appropriate transversality hypotheses is satisfied.

Then there exists a stable MMO with signature 1^{k+1} .

Theorem 6.3 (Stable MMOs with signature 1^i ?)

Suppose system (52) satisfies assumptions 1. - 4. of Theorem 6.2 and, the following additional assumption:

- For $\delta = 0$, the global return point is on the singular strong canard $\bar{\gamma}_s$ and as δ passes through zero the return point crosses $\bar{\gamma}_s$ with nonzero speed.

Suppose now that $\delta = O(\epsilon^{(1-\mu)/2}) > 0$. Then, for sufficiently small $0 < \epsilon \ll 1$ and $k \in \mathbf{N}$ such that $2k + 1 < \mu^{-1} < 2k + 3$, the following holds. For each $i, 1 \leq i \leq k$, there exist subsectors $\bar{I}_i \subset I_i$ with the corresponding distance intervals (δ_i^-, δ_i^+) of widths $O(\epsilon^{(1-\mu)/2})$, which have the property that if $\delta \in (\delta_i^-, \delta_i^+)$, then there exists a stable MMO with signature 1^i .

Theorem 6.2 is rather technical, stating the existence of the global return under certain circumstances, when the trajectory has entered the rotational sector I_{k+1} , meaning, close to the weak primary canard and undergoing $k + 1$ SAOs. Since the width of this sector is $O(1)$ and therefore much larger than the width of the other sectors that trajectories can enter into, we would expect more trajectories undergoing $k + 1$ SAOs than i SAOs, where $i \in 1, \dots, k$. However, Theorem 6.2 requires $\epsilon^{1/2} \ll \mu$ and since $\epsilon \ll 1$, we must have $\mu \approx 1$ in order to apply the results in this theorem (as $0 < \mu < 1$). This

is not commonly observed in practice and therefore, the logical conclusion is to investigate whether a global return mechanism exists for the other I_i , for $i \leq k$. The existence of these MMOs is discussed in Theorem 6.3. Theorem 6.3 introduces δ which corresponds to the distance between γ_s and the trajectory that has entered the funnel region.

As introduced in the beginning of Section 6, the signatures of MMOs are represented in terms of the number of large amplitude oscillations ($L_1 L_2 \dots$) and the number of small amplitude oscillations ($s_1 s_2 \dots$), and the conventional notation is $(L_1^{s_1} L_2^{s_2} \dots)$. In the case of the folded node, under the conditions of the theorems, we have a rather straightforward signature. The first theorem states the existence of the signature 1^{k+1} , where $L_1 = 1$ and $s^1 = k + 1$, and equivalently, the second theorem in this chapter discusses MMOs with signature $1^i, i < k$. The dynamics due to a folded node are well understood, however, there exist more complex dynamics for other types of equilibria and singularities. To illustrate this, one of these cases is briefly introduced in the next section.

6.2 Singular Hopf Bifurcation

If the folded singularity is of saddle node type, as introduced in Section 5, there is further classification possible. There exists the saddle node of type 1, in which the folded singularity coincides with the equilibrium of the desingularised reduced system, which is not the equilibrium of the full system. However, when the parameters of the system coincide in such a way that an equilibrium of the full system and a fold point coincide, then the folded saddle node is said to be of type 2. If a saddle-node of type 2 occurs for a specific parameter regime, then a singular Hopf bifurcation arises at $O(\epsilon)$ distance from the equilibrium, and is defined as follows:

Definition 6.4. *Singular Hopf Bifurcation ?*

A singular Hopf bifurcation occurs at a certain parameter regime in the system which is $O(\epsilon)$ away from a saddle-node of type 2. There, the eigenvalues of the system cross the imaginary axis, therefore they have a zero real part. Then small oscillations, called limit cycles occur in the system. There are two types of singular Hopf bifurcation. A supercritical Hopf bifurcation occurs when a stable limit cycle arises from an unstable equilibrium point, while a subcritical Hopf bifurcation causes unstable limit cycles to appear around a stable equilibrium.

A second equilibrium of focus type can appear close to the fold and interact with the folded saddle node of type 2. Depending on the parameter regime of the system, this gives rise to various different dynamics. The normal form, which allows for global return mechanisms, due to its S-shaped slow manifold, is the following,

$$\begin{aligned}\epsilon \dot{x} &= y - x^2 - x^3, \\ \dot{y} &= z - x, \\ \dot{z} &= -\nu - ax - by - cz.\end{aligned}$$

There exist stable MMOs for some parameter values, where ν is small and the orbit for a specific choice of such parameters is displayed in Figure 19c. Other parameter regimes may give rise to more complex orbits, for example chaotic trajectories that will, with decreasing ν , turn into a small-amplitude chaotic attractor. An example trajectory is displayed in Figure 19a, and the time series of this trajectory is displayed in Figure 19b. The characterisation of the dynamics of this system for different parameter regimes is still ongoing, and there exist only classifications for certain parameter regimes of ν .

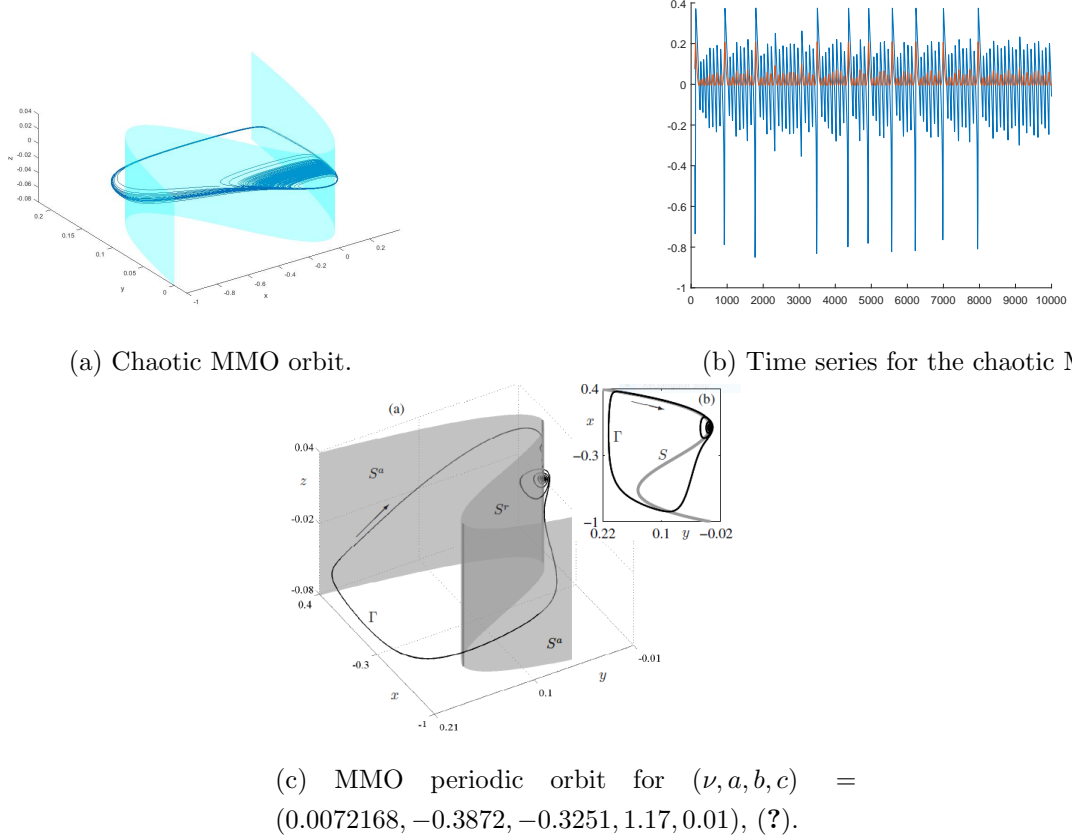


Figure 19: Orbits associated with mixed mode oscillations (?).

7 Discussion

We have shown that to fully explain the dynamics of a fast-slow system, standard Geometric Singular Perturbation Theory is not sufficient, due to the lack of normal hyperbolicity at some points. To remedy this, these points were treated using Blow-Up analysis, so that ‘enough hyperbolicity’ was gained to apply GSPT. This allowed a full explanation of the global dynamics in the system, as long as there were no bifurcations present. In the neighbourhood of $\lambda = 0, 2$, a Hopf bifurcation was shown to occur, fundamentally changing the dynamics and introducing small amplitude oscillations as opposed to the large amplitude relaxation oscillations seen in other cases. This was caused by a trajectory existing that joined the attracting manifold to the repelling manifold. The manifold splits under perturbation in either λ or phase space. The nature of the split determines the amplitude of the oscillations, and the dynamics around the fold point leading to canards with or without heads. In the planar case, these canard solutions only occur in an exponentially small region of the fold point and so an additional slow variable was introduced to produce more persistent canard trajectories. We then showed how in certain cases this leads to mixed mode oscillations and even chaotic systems.

This approach is widely applicable to fold points in the planar case and folded nodes in the three dimensional case. However, it does not complete the analysis of fast-slow systems. If a Hopf bifurcation occurs close to a folded saddle of type II, the two interact in a way that is not yet fully understood. Further extension is possible in simulating such fast-slow systems as their stiffness and small scale pushes the limits of standard numerical methods.

Mixed mode oscillations are an important area of study, as they model a wide range of biological phenomena. Interesting avenues to be pursued in this area include application of the theory to the Hodgkin-Huxley model of coupled neurons and the Koper model, see for example ?.

8 Acknowledgements

We wish to thank our advisors Nikola Popovic and Mariya Ptashnyk for their patience and guidance throughout the project. We also wish to thank Panagiotis Kaklamanos for many conversations clarifying concepts and ideas. The authors were supported by The Maxwell Institute Graduate School in Analysis and its Applications, a Centre for Doctoral Training funded by the UK Engineering and Physical Sciences Research Council (grant EP/L016508/01), the Scottish Funding Council, Heriot-Watt University and the University of Edinburgh.

8.1 Author Contribution

Throughout this project we were able to carry out work on the *Interactions Between Fast and Slow Dynamics in Nonlinear Evolution Equations*. From the beginning of the project we worked collaboratively

8. ACKNOWLEDGEMENTS

to keep each other up to date on the various areas of mathematics, without diverging significantly from each others area of focus. This resulted in an equal weighting in the work presented in the following project as all authors engaged in healthy debate on what work should be included and the way in which the project is written. However, Kieran continued on the analysis of the canards while Thomas and Jonna moved onto mixed mode oscillations. Although this was the case, all three authors were actively involved in editing and expressing ideas during this divergence of work. Therefore it is reasonable to conclude that equal weighting should be applied to all authors.

A Numerical Simulation

In this appendix, we will give a brief tutorial on the use of MATLAB to produce plots like those seen in the project. Fast-slow systems like the ones studied here are a classic example of *stiff* ODEs^a.

Definition A.1 (Stiffness Ratio). *Consider $\dot{x} = F(x)$ where $x \in \mathbf{R}^n, F \in C^r(\mathbf{R}^n, \mathbf{R}^n)$. Let*

$$x' = Ax, \quad A \in \mathbf{R}^{n \times n}$$

denote its linearisation. Suppose all the eigenvalues λ_j of A have negative real parts. Then the stiffness ratio, μ is defined as

$$\mu := \frac{\max_j(\operatorname{Re}(\lambda_j))}{\min_j(\operatorname{Re}(\lambda_j))}$$

If μ is large, the system is called stiff.

Stiffness is not a well-defined concept, it can be seen as a general term for a set of equations which are difficult to solve numerically to a high level of accuracy. Throughout this section we will consider the general problem above as an initial value problem.

$$\begin{cases} \dot{x} = F(x) \\ x(T_0) = x_0 \end{cases}$$

As before, $x \in \mathbf{R}^n$ and $F \in C^r(\mathbf{R}^n, \mathbf{R}^n)$. To solve such a system numerically, time must be discretised. Using standard notation, let h be the time step between points on the solution. To differentiate between the continuous solution $x(t)$ and the discretised solution, we denote the latter by $x(t_j) = x_j$. Here $t_j = T_0 + jh$. As a first example, consider the modified Euler method.

$$x(t_{n+1}) = x(t_n) + hF\left(x(t_n) + \frac{1}{2}F(x(t_n))\right)$$

Or, in the more compact notation,

$$x_{n+1} = x_n + hF\left(x_n + \frac{1}{2}F(x_n)\right)$$

This is a simple method and provides a starting point in considering error between true and numerical solutions.

The go-to ODE solver in MATLAB is `ode45`. This function uses the Dormand-Prince Runge-Kutta method, an explicit single-step formula. The Runge-Kutta method (RK4) is similar to the explicit Euler method in that it calculates the next point (x_{n+1}) using only its current value (x_n). Unlike the Euler method however, it yields much lower error by using a better approximation of the derivative at points in between x_n and x_{n+1} as opposed to only the derivative at the initial point. The Runge-Kutta method uses the following relation.

^aIndeed, the MATLAB documentation for its stiff solver, `ode15s`, uses the Van Der Pol equation as it's example.

$$x_{n+1} = x_n + \frac{1}{6}h(k_1 + 2k_2 + 2k_3 + k_4)$$

where

$$\begin{aligned} k_1 &= F(x_n) \\ k_2 &= F\left(x_n + \frac{1}{2}hk_1\right) \\ k_3 &= F\left(x_n + \frac{1}{2}hk_2\right) \\ k_4 &= F(x_n + hk_3) \end{aligned}$$

The Runge-Kutta family of solvers are ubiquitous in numerical analysis, and most methods can be categorised as belonging to this set of methods. Even the simplest, the explicit Euler scheme, is a RK method. Note that `ode45` doesn't use RK4, it uses an adaptive method that repeats steps if the error in the step is too high. This produces an even more accurate solution without adding much computational cost.

Let's look at the use of these various methods on the simplest fast-slow system.

$$\begin{cases} \begin{pmatrix} \dot{x} \\ \dot{y} \end{pmatrix} = \begin{pmatrix} -1/\epsilon & 0 \\ 0 & -1 \end{pmatrix} \begin{pmatrix} x \\ y \end{pmatrix} \\ (x(0), y(0)) = (x_0, y_0) \end{cases} \quad (63)$$

This system has an easy analytic solution, $x(t) = x_0 \exp(-t/\epsilon)$, $y(t) = y_0 \exp(-t)$. For this reason it is a useful test system with which to analyse the convergence of numerical schemes. The stiffness ratio for this system is

$$\mu = \frac{\max_j(\operatorname{Re}(\lambda_j))}{\min_j(\operatorname{Re}(\lambda_j))} = \frac{1}{\epsilon}$$

The time separation, $\epsilon \ll 1$ and so this system is very stiff. We thus expect explicit solvers to perform poorly. The lack of stability of these algorithms in practice, even for very simple systems, clearly necessitates the introduction of alternative methods.

A.1 Stiff Solvers

MATLAB offers a number of solutions to this problem. It has four inbuilt stiff solvers: `ode15s`, `ode23t`, `ode23s` and `ode23tb`. Here we look at the first three and compare them with the standard `ode45`. These use a variety of methods to outperform the standard RK4 method. In Figure 20, `ode45` would have obtained the solution to a similar accuracy. This is because if the error is outside of a predefined tolerance, it repeats the step with a smaller step size. Although the solution is the same the cost here is in computational efficiency. This is true for all the stiff solvers, as Figure 21 shows. It is worth testing each stiff solver on the problem at hand to find the most efficient solver. This will depend on the

A. NUMERICAL SIMULATION

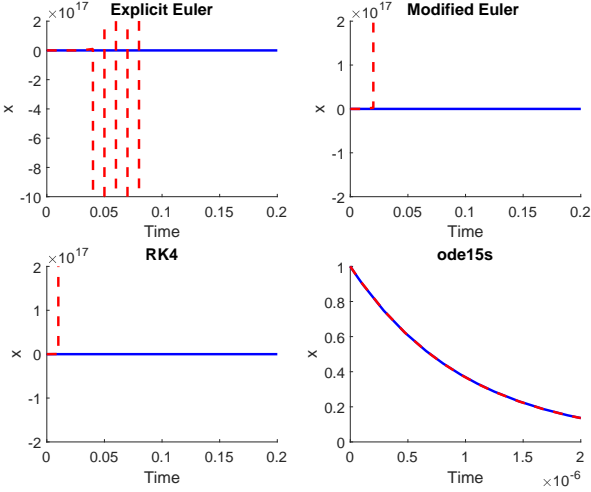


Figure 20: Comparison of stability of different numerical schemes applied to Equation 63. Blue solid line indicates analytic solution, dashed red indicates numeric solution using the scheme given in the plot title. Note the varying scales on the axes.

Algorithm	ode45	ode15s	ode23t	ode23s
Successful Steps	2.6971×10^7	5727	6186	6506
Failed Attempts	6.41547×10^6	2529	2103	1105
Function Evaluations	2.00319×10^8	19391	22437	34752
Elapsed Time (s)	250.957128	1.021033	2.250413	0.579021

Table 1: Comparison of MATLAB's stiff solvers applied to the Van der Pol system (4)

form of the problem and the method each solver implements. Table (1) gives some statistics for the efficiency of each solver when applied to an incredibly stiff Van der Pol system (4) with $\epsilon = 1 \times 10^{-6}$ and $\lambda = 1$. Despite `ode45`'s accuracy, we can see it pales in comparison to any of the stiff solvers. The table shows `ode23s` to be the quickest, although it does evaluate the function many times it rarely fails a step. For this reason, this algorithm was chosen to produce the figures throughout this report. This however is still not the optimal method of computation. More complex solutions to boundary value problems can be created on each of the branches before being joined together to create a full image.

The MATLAB code used to produce the figures in this report is available on line at <https://github.com/Tom271/FastSlowDynamics/tree/master/Code>.

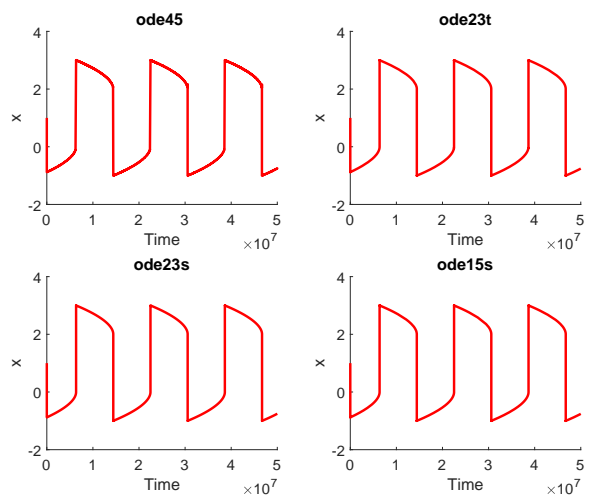


Figure 21: Comparison of stiff solvers for VDP for $\epsilon = 1 \times 10^{-6}$, $\lambda = 1$. All solvers obtain the correct solution.